Durham E-Theses

Tau-p mapping and interpretation of seismic reflection data from the western Isles region of Scotland

Lambert, Mark E.

Tau-p Mapping and Interpretation of Seismic Reflection Data

from the Western Isles Region of Scotland.

Mark E. Lambert.

Department of Geological Sciences,

University of Durham.

September, 1982.

A thesis submitted as part requirement for the degree of

Master of Science.

ABSTRACT

Seismic data are conventionally recorded, processed and displayed in the X-T domain, where X is the source-receiver offset and T is the two-way traveltime. There are advantages, however, in mapping the same data in a different domain; that of intercept time τ and horizontal ray parameter p. Computer programs written for performing the transformation from X-T to τ-p were adapted for use with marine data acquired in the western Isles region of Scotland in order to obtain information about the velocity structure in that area. The results obtained are compared with those produced by the more conventional methods of refraction surveying and it is found that the data are of insufficient quality to facilitate a geological interpretation to be made with the τ-p method alone and that the method is of no use with the poorest quality data. Recourse to the conventional methods is found to be necessary, and the results obtained verify previous results from other work.

CONTENTS

INTRODUCTION

The seismic method of exploration is based on recording the response with time of the subsurface to excitation. Consequently, methods of analysis and interpretation have developed around the observational parameters that may be controlled or monitored: these are the source-receiver offset X, and the two-way traveltime T.

Modern techniques of wide-aperture, multichannel, marine seismic data acquisition to investigate deep crustal structure (Savit, 1977; Stoffa and Buhl, 1980) have resulted in data sets that include both wide-angle reflections and refractions. In shallow crustal studies (hydrocarbon exploration, for example) it is standard practice at the processing stage to mute the refracted arrivals, as it is only the near-vertical incidence reflections which are of interest. In deep ocean seismic surveys, such as deep crustal studies, it is the refracted arrivals which are easiest to obtain. Usually reflections and refractions are treated differently, even when they are both present in the same data set. It would be preferable from the viewpoints of scientific elegance and practicality, if there existed a method of interpretation that could be applied to both types of arrival simultaneously. This appears difficult to achieve in the X-T plane, primarily because of the fact that for refraction work, T may be a multi-valued function of X.

A new plane which is able to unfold the multiplicities in X-T refraction data by virtue of being a single - valued function of an independent parameter has been suggested by Gerver and Markushevich (1966). The new dependent parameter is the intercept time τ . The ray parameter p may be defined as the inverse of the horizontal phase velocity, or horizontal slowness and by Snell's law may be shown to remain constant along the ray. The intercept time τ , is the value of the intercept on the time axis of a tangent to the traveltime curve of gradient p.

Map 1

MARINE GEOLOGY of the MALIN/
HEBRIDEAN SEA REGION

Tertiary Plutonic Centres
Tertiary Lavas of Mull & Rhum
Mesozoic Sediments undiff.
New Red Sandstone
Old Red Sandstone
Caledonian Granite
Dalradian Metamorphics
Moinian   "
Torridonian
Lewisian
Basement uncertain   ? ?
Moine Thrust

LOCATION

57°N

56°30'

SEA of the
HEBRIDES TROUGH.

HAWES
BANK

BARRA
TROUGH

Outer Hebrides Fault

MINCH FAULT

MULL

TIREE BLOCK

Skerryvore
Trough

SKERRYVORE FAULT

V. Thick drift on a
Tertiary & Mesozoic
Sequence

STANTON
BANKS BLOCK

BLACKSTONES
BANK (?Cret.)

minor
intrusives
in disturbed
Mesozoic
sediments

Dubh Artoch Fault

COLONSAY BASIN

JURA

MALIN BASIN

CHAPTER 1

1.1. Introduction

The location of the survey area is between the Outer Hebrides and the Inner Isles of Coll, Tiree and Rhum, with particular emphasis on the Skerryvore and the Sea of the Hebrides troughs. A map of the marine geology is shown (map 1). Seismic reflection surveys were conducted along the tracks shown in figures 17 and 18, and the locations along the lines from which data were used for this work are indicated by the file numbers shown on the computer print-outs. The locations were selected so that study of three major rock types was possible. These were the Lewisian complex, the Mesozoic sediments and the Torridonian basement.

Maps showing the marine geology of the area are given by Binns et al (1974), and Uruski (pers. comm.) from whom map 1 is taken. All of the rock types described below outcrop enabling field observations to be made. Full accounts of the rock types encountered on the Inner Isles are given by Peach and Horne (1930), Richey and Thomas (1930) and Harker (1941).

1.2. Geology

The major controlling factors on the geology in the region are the Minch, the Skerryvore and the Great Glen (or Dubh 'rtach) faults which run approximately north-east to south-west. The Minch and Skerryvore faults form the western margin of two asymmetric troughs that are filled with Upper Palaeozoic and Mesozoic sediments underlain by Precambrian and Lower Palaeozoic rocks.

There has been subsequent Tertiary igneous activity and cross-faulting that has had considerable effect on the geology, the most obvious result perhaps being the lava flows of Mull and Skye. It is

this cross-faulting as well as tilting of the faulted Sea of the
Hebrides trough that causes the older basement rocks to outcrop in
places.

The older rocks are covered by a relatively thin layer of younger
sediments with the facies distribution being primarily dependent on the
water depth, the degree of exposure to the prevailing south-westerly
swell and the relief of the bedrock surface.

The rock types investigated are given below in chronologically
ascending order.

1.2.1.   The Lewisian Complex.

The Lewisian complex is an extensive formation in north-west
Scotland that forms a basement of metamorphosed, intrusive igneous
rocks which are mainly gneisses and highly metamorphosed sediments.
The older sedimentary formations may be classified as being Pre-
Lewisian and include pure and impure calcareous rocks in addition to
some pelites and some psammites.   The gneisses were collectively
termed the Lewisian gneiss by the Geological Survey and apply to the
system of rocks that form the basement over which the Torridonian
sediments were laid down.   The rocks that constitute the Lewisian
gneiss are Precambrian and are mainly coarse-grained, outcropping
extensively in the north-west Highlands, parts of the Inner Hebrides
and almost all of the Outer Hebrides to result in a complex of
gneisses that were formed by a series of plutonic intrusions.   They
range from the oldest ultrabasic through to basic and intermediate,
to the youngest, acidic rocks.   The older basic rocks show minera-
logical conversion, such as the altering of pyroxene to horneblende,
as well as alteration due to the presence of later, acidic °
intrusions.

It was Hutton who originally proposed that the Lewisian gneiss was formed by the crystallisation of sedimentary formations by the action of heat, although this interpretation is now believed to be inaccurate in certain locations.

The rock types that comprise the Lewisian gneiss are banded, and may thus be distinguished and classified as orthogneisses, paragneisses, grey orthogneisses and dark orthogneisses.

Other categories of rock types common in the Lewisian gneiss are feldspar-free rocks, calcified orthogneisses and the younger, coarse pegmatites .

1.2.2.   The Torridonian

The Torridonian sequence is composed of Precambrian red sandstones, grits, conglomerates and breccias that lie unconformably on the Lewisian gneiss.   The arenaceous rocks that constitute this sequence were named 'Torridonian' by Nicol, who succeeded in distinguishing them from the Old Red Sandstone formation of the Silurian and Devonian.   They outcrop extensively around Loch Torridon in west Ross-shire as well as on Rhum and Skye.   In the lower parts are flaggy or shaly beds that are succeeded by grey grits with the bulk of the thickness being due to arkoses that are often coarse with pebbly bands.   These sediments are believed to have been laid down in continental conditions and the divisions of the Torridonian are described by the Geological Survey and are the Diabaig group, the Applecross group, and the Aultbea group, in ascending order.

1.2.3   The Mesozoic Sediments

This group of sediments lie unconformably on the earlier

formations and have remained relatively protected from erosion by the

overlying Tertiary lavas.   The youngest of the Mesozoic rocks

constitute a major part of the Sea of the Hebrides trough, and attain

thicknesses of up to three kilometres in places (Binns et al, 1974).

The sequences that make up the rather complicated Mesozoic

geology are given below in ascending order.

(a)   Lower and Middle Triassic

This group consists of thin beds of red sandstones and cornstones

with conglomerates and breccias.   It rests unconformably on the Moine

Schists and is found to be best preserved in down-faulted basins and

hollows.

(b)   Upper Triassic

This group is comprised of thin beds of sandy or calcareous

limestones with some yellow sandstone present.

(c)   Lower Jurassic.

This group contains two distinct rock types:

(i) Broadford Beds:- the lower division of the Lower Jurassic.

The beds are mainly calcareous, consisting of hardened shales and thin

beds of compact limestone.

(ii)   Pabba beds:- a thick series of sandy, well-bedded shales

containing scattered flakes of white mica.

Both types are particularly fossiliferous in places.

(d)   Middle Jurassic

White, fine-grained and well-bedded sandstones make up this group.

The beds are well baked in places showing no evidence of fossils.

(e)   Upper Jurassic

Included in this group are fine-grained, black, fissile shales,

calcareous shales, mudstones, fossiliferous limestones and yellow or

red sandstones.

UNCONFORMITY

(f)   Upper Cretaceous

This group is represented by a thin series of marine deposits and white, desert sandstone, with some chalk present, that rests unconformably on the eroded Jurassic surface.

CHAPTER 2

2.1. Historical Background of the Tau-p Method

The derivation of ray parameter p, in terms of T and Δ , the angular distance, from a spherically stratified earth model and the inversion of observational data to give velocity distributions as given by Bullen (1963) is a useful starting point to an account of the history of the method.

The function $\tau(p) = T(p) - pX(p)$, is introduced by Gerver and Markushevich (1966) in their formulation of the solution of the problem of determining the velocity-depth function from traveltime curves, which is a generalisation of the Herglotz-Wiechert method (Herglotz, 1907; Wiechert, 1910) to a medium with low-velocity zones.

Gerver and Markushevich (1967) state the conditions required for the existence of a unique solution to the inverse problem, except in the low-velocity zones themselves. The conditions are that an infinite amount of perfectly accurate traveltime data at all distances from sources above and below all the low-velocity zones is present.

Given a finite amount of data, Backus and Gilbert (1967) show that the number of velocity profiles that fit the measured data is either zero or infinite, and they also provide a method of selecting suitable profiles that is not affected by many of the limitations of the Herglotz-Wiechert method, as well as considering observational errors. Following the arguments of Brune (1964), it may be shown that errors in $\tau(p)$ due to errors δp, in p are of second order in δp.

Taner and Koehler (1969) describe a method of estimating r.m.s. velocities by employing hyperbolic searches for semblance among appropriately gathered arrays of traces and discuss the principles

for calculating velocity spectra displays.

Johnson and Gilbert (1972) apply the function to a linear-
ised inversion method and use it to examine core and mantle velocity
structure using teleseismic ray data.

Bessonova et al (1974) use the tau method for inversion of
traveltimes obtained from deep seismic sounding data by assuming
spherical symmetry and a lower limit for the velocity in low-
velocity zones (from the results of Gerver and Markushevich, 1966).
Bessonova et al (1970) also consider the transformation of limits
for $\tau(p)$ into limits for $Y(p)$ - the velocity-depth function, and
also obtain estimates of $\tau(p)$ from given traveltime data using their
graphical method of parallelograms.

A different method of estimating $\tau(p)$ from traveltime data is
introduced by Bates and Kanasewich (1976). For each branch of the
traveltime curve, they fit T observations to a family of second
order polynomials in X and then map the curves into the τ-p plane.
The method is modified to handle reflection data by Kennett (1977)
whose method also allows bounds to be placed on the velocity-depth
function in the reflecting region.

Diebold and Stoffa (1979) develop the exact form of the common
mid-point traveltime equation in terms of X, τ and p, and show that
the resulting equation is valid for all vales of X. They also show
that the inherent averaging of slowness in a multi-layered example
in their formulation gives rise to distinct advantages over other
methods in the presence of dip as well as presenting a method of
deriving a velocity-depth function which is applicable to both reflect-
ed and refracted arrivals. This method is particularly relevant
with respect to modern techniques of wide-angle, multichannel,
seismic data acquisition where data sets containing wide-angle reflect-
ions and refractions have been obtained (Stoffa and Buhl, 1980). For

the large offsets present in this form of data set the more conventional methods of velocity analysis are invalid.

Direct mapping of data in the X-T plane to the τ-p plane is achieved by Stoffa et al (1979) who uses wave stack and semblance calculations across common mid-point gathers. Semblance is also used to derive a windowing filter to eliminate aliasing by setting an arbitrary threshold level of semblance below which the data are muted.

Bowen (1980) suggests that this method of choosing arbitrary thresholds is unsatisfactory, and describes a modification to the 'anti-aliasing stack' calculation by automatically excluding aliased portions of the summation trajectories from the stack. This more elegant method is shown to produce less waveform distortion and better alias discrimination.

2.2. The General Form of the Traveltime Equation

The following is a brief account of the basic principles and assumptions of the τ-p transformation. A more formal and detailed account is given by Diebold and Stoffa (1979) from which the following summary is taken.

The most general form of the traveltime equation is developed and is shown to be equally valid for reflections and refractions, as well as for all values of offset and all commonly used experimental geometries.
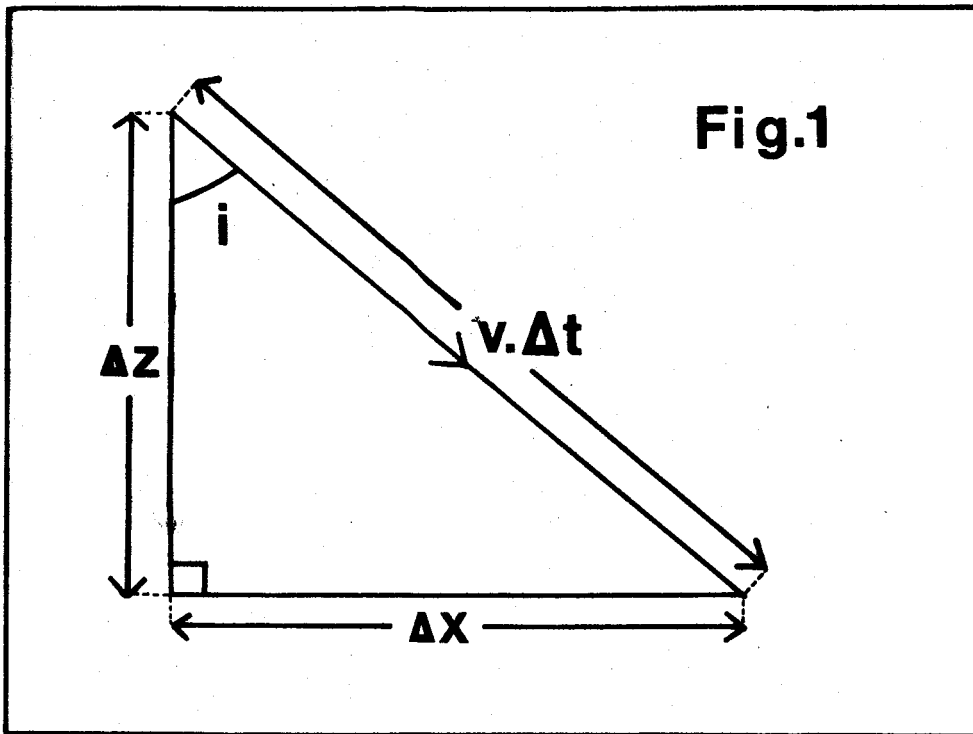
Consider a plane wave travelling in a homogeneous medium of velocity v as shown in figure 1.

The total distance travelled in time $\Delta t = v\Delta t$

Resolving the distance into components yields

$\Delta X = v \ \Delta t \sin i \quad (1)$ and

$\Delta Z = v \ \Delta t \cos i \quad (2)$

Fig.1

The traveltime may also be resolved into component form:

$$\Delta t = p\ \Delta X + q\ \Delta Z \qquad (3)$$

$$\text{where } p = \sin i / v \qquad (4)$$

$$\text{and } q = \cos i / v \qquad (5)$$

Here, p is the horizontal ray parameter, or horizontal slowness, and q is the vertical ray parameter, or vertical slowness ('slowness' is equivalent to the inverse of velocity).

If the slowness of the wave is u, where

$$u = 1/v,$$

then it is simple to show that

$$u^2 = p^2 + q^2 \qquad (6)$$

Substituting for v from equations 4 and 5 into equations 1 and 2 yields

$$p\ \Delta X = \sin^2 i\ \Delta t \qquad (7) \qquad \text{and}$$

$$q\ \Delta Z = \cos^2 i\ \Delta t \qquad (8)$$

combining equations 7 and 8 produces

$$p \Delta X + q\ \Delta Z = \Delta t \qquad (9)$$

If a stack of n homogeneous, horizontal layers of thickness Z_i is considered, then the total two-way traveltime may be expressed as the sum of contributions from each layer (figure 2).
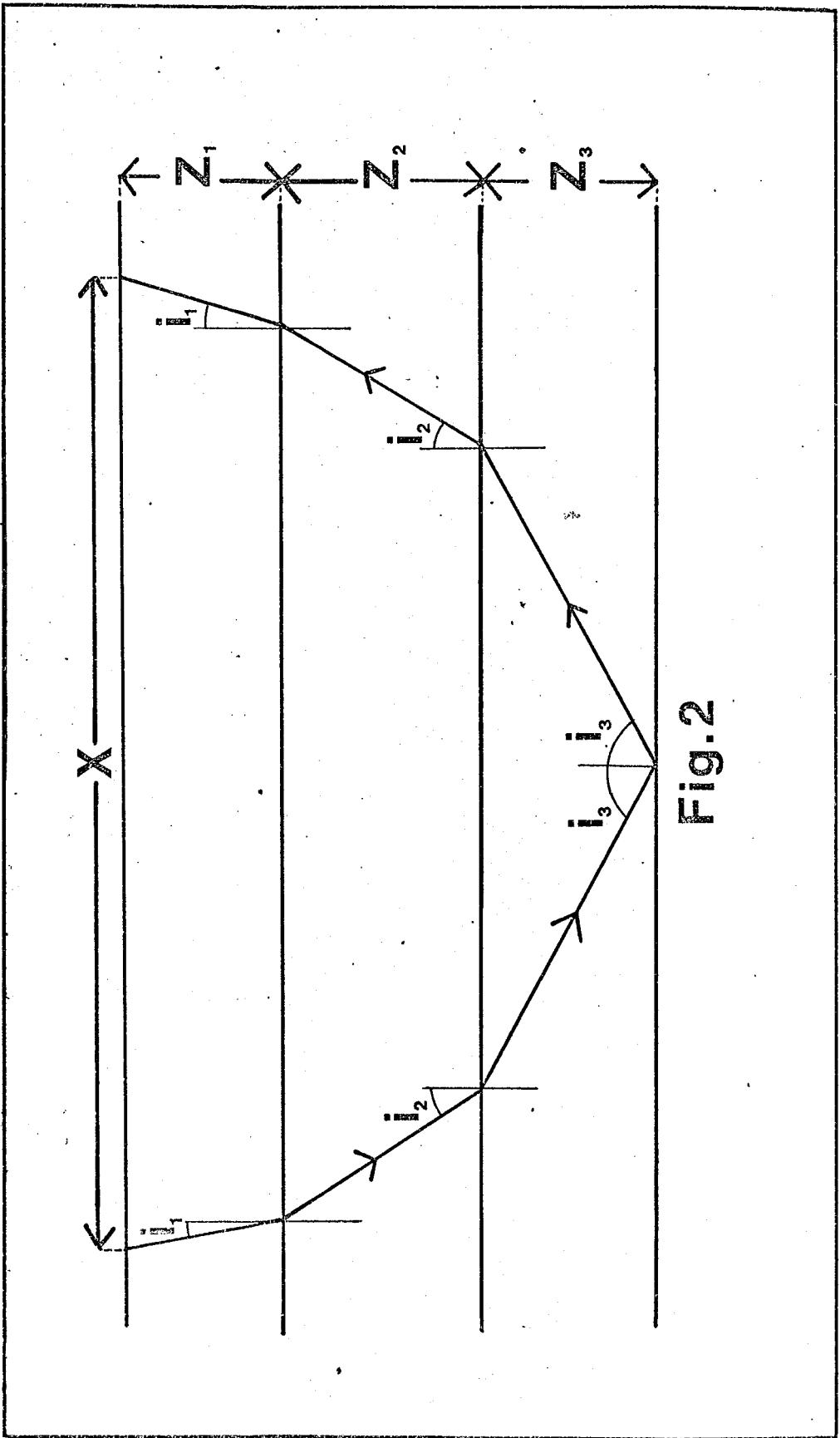
Fig.2

i.e. $\quad T = 2\sum_{i=1}^{n} \Delta t_i$

$\qquad = 2\sum_{i=1}^{n} \; (p_i \Delta X_i + q_i \, Z_i) \qquad\qquad (10)$

From Snell's law, it may be shown that p is constant for waves

across a horizontal interface since

$\qquad \sin \; i_1 \; / v_1 \; = \; \sin \; i_2 / v_2 \qquad$ and therefore

$\qquad\qquad p_1 \; = \; p_2 \qquad\qquad\qquad (11)$

Therefore equation 10 may be re-written as

$\qquad\qquad T \; = \; pX + 2\sum_{i=1}^{n} \; q_i \, Z_i$

$\qquad\qquad\quad = \; pX + \tau \qquad\qquad (12)$, where

$\qquad\qquad \tau \; = \; 2\sum_{i=1}^{n} \; q_i \, Z_i \qquad\qquad (13)$

Equation 12 is the equation of a straight line in the X-T

plane with gradient p and intercept time τ , which is tangential

to the traveltime curve at the point (X,T). It is valid for all

reflections and refractions.

For a single layer case equation 13 simplified to

$\qquad \tau \; = \; 2qZ$

$\qquad\quad = \; 2Z \; (u^2 - p^2)^{1/2} \qquad\qquad (14)$

consequently, the contribution to τ from a single layer may be

written as

$\qquad \tau_i \; = \; 2Z_i \; (u_i^2 - p^2)^{1/2} \qquad\qquad (15)$

The physical meaning of τ is now recognisable as the aggregate

of vertical slowness-thickness products as described by Bessonova

(1974). It is clear that all information about layer thicknesses

is contained in τ.

Equation 15 describes an ellipse in the τ-p plane. This may be

readily shown as follows:

$\qquad \tau_i^2 \; = \; 4 \, Z_i^2 (u_i^2 - p^2)$

$\qquad \Rightarrow \; 1 \; = \; p^2/u_i^2 + \tau_i^2/4Z_i^2 u_i^2 \qquad\qquad (16)$

For the single layer case,

$$\tau_1(0) = 2qZ$$

where $\tau(0)$ is the two-way, normal incidence traveltime for the single layer. (The horizontal phase velocity is zero for normal incidence). Thus equation 16 may be re-written as

$$p^2/u_1^2 + \tau_1^2/\tau_1^2(0) = 1 \qquad (17)$$

where $\tau_1(0)$ and u_1 are the semi-minor and semi-major axes respectively.

For the quadrant defined by positive τ and p, one quarter of a complete ellipse is mapped, as shown in figure 3.
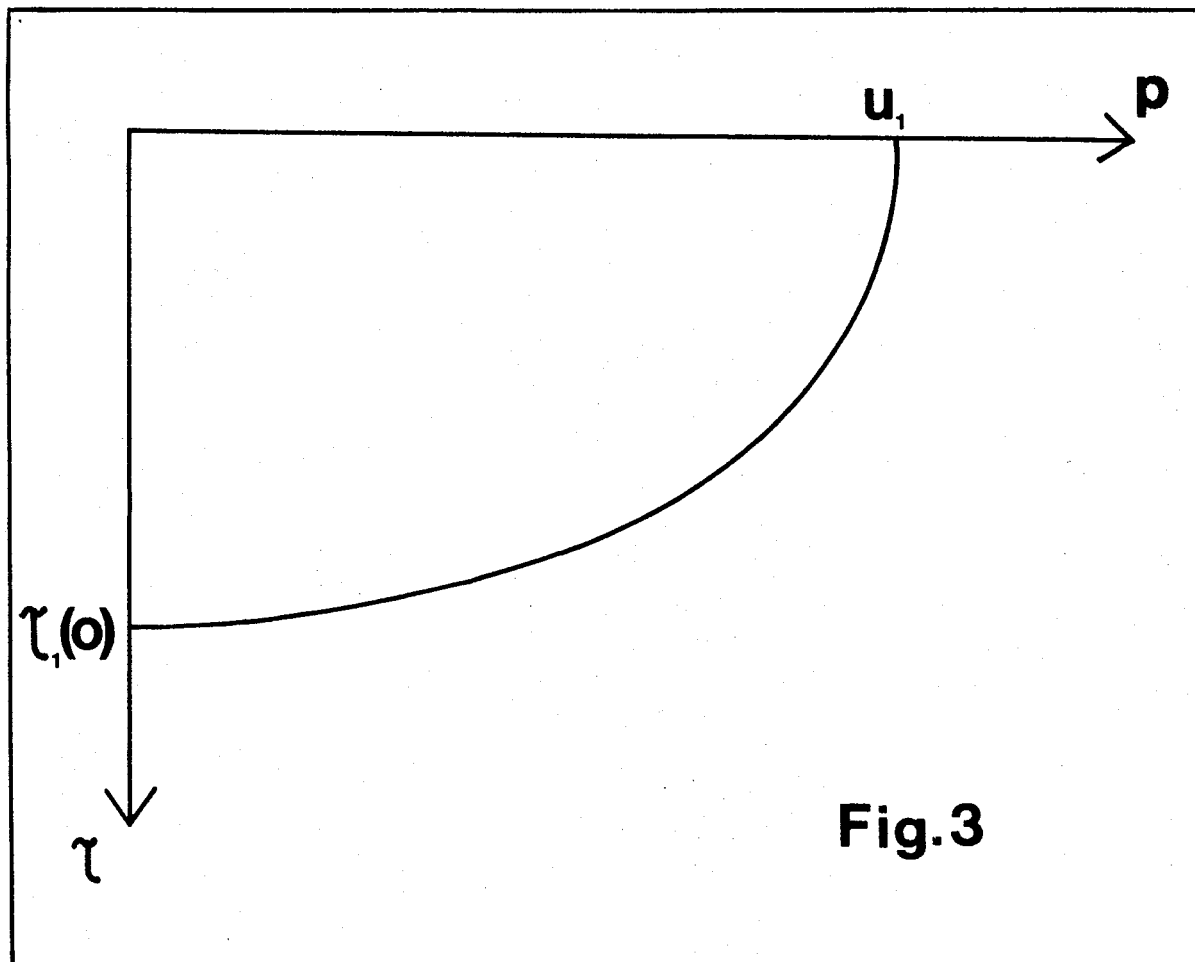

Fig.3

For the multi-layered case each layer may be considered as contributing one quarter of an ellipse to the curve in the τ -p

plane. The ellipses are then summed to give the complete trajectory. A typical, three-layer case is shown in figure 4.

The wide-angle reflections are characterised by high energy arrivals as little energy escapes into the lower layers. This leads to the well-defined outer limits.

From equation 12 it is apparent that

$$d\tau/dp = - X \qquad (18)$$

So, for normal incidence,

$$d\tau/dp = 0 \qquad (19)$$

For a horizontally propagating wave (at grazing incidence), the condition is

$$dp/d\tau = 0 \qquad (20)$$

2.3 The Effect of Dipping Layers

In the presence of dip, the form of the general traveltime equation is modified (Diebold and Stoffa, 1979) and may be written as

$$T = X_a p_a + X_b p_b - \sum Z_i (q_{ai} + q_{bi}) \qquad (21), \text{ where}$$

$p_a = \sin a_1/v_1$; $p_b = \sin b_1/v_1$; $q_{ai} = \cos a_i/v_i$; $q_{bi} = \cos b_i/v_i$

An example of a possible structure for which this equation is applicable is shown in figure 5, and a complete derivation is given in Diebold and Stoffa (1979).

Using the common-depth-point, or C.D.P., geometry as in figure 5 where sources and receivers progress at equal speed in opposite directions whilst maintaining a common mid-point is advantageous over the use of common source or common receiver arrays because the inherent averaging of up-dip and down-dip slownesses in the traveltime equation leads to greater accuracy in the determination of the velocity-depth function.
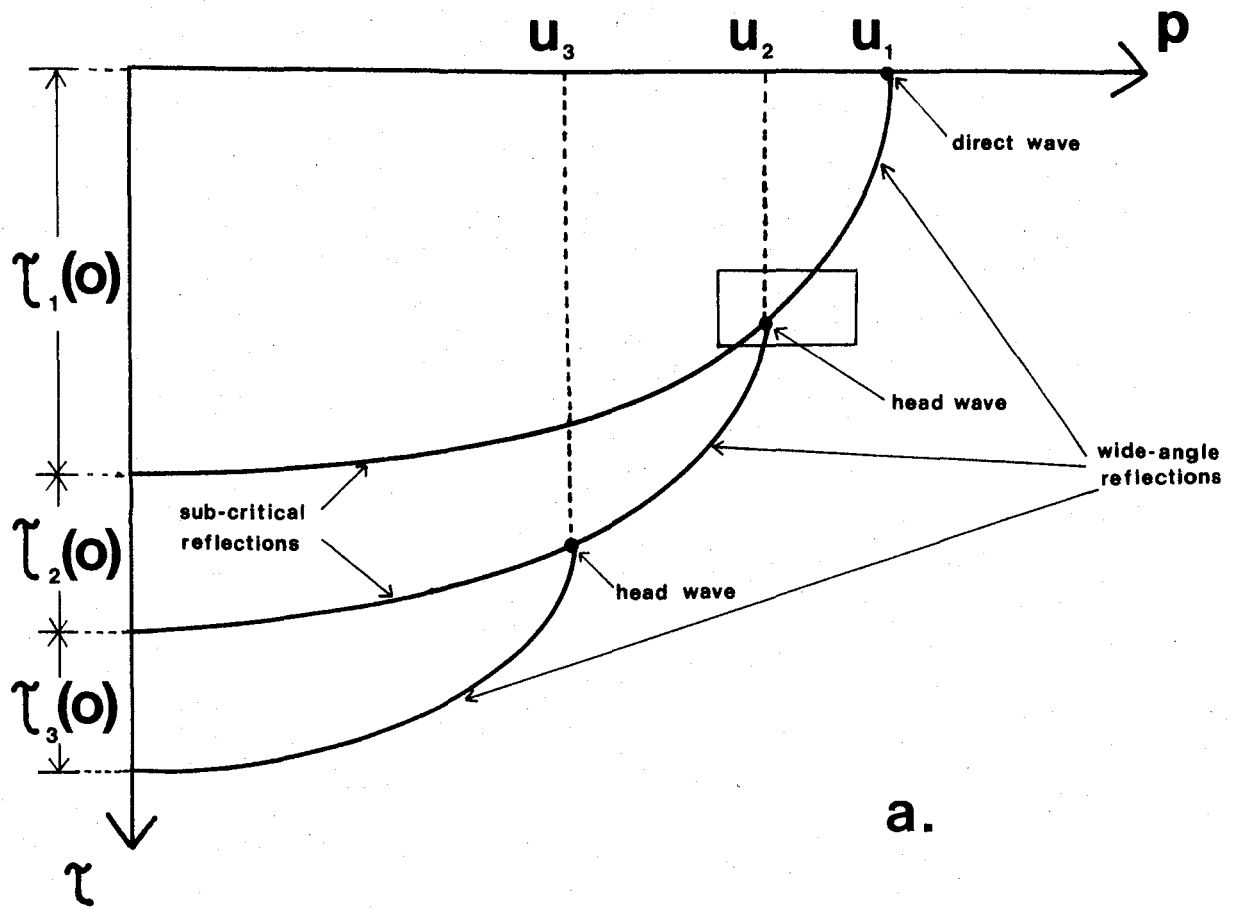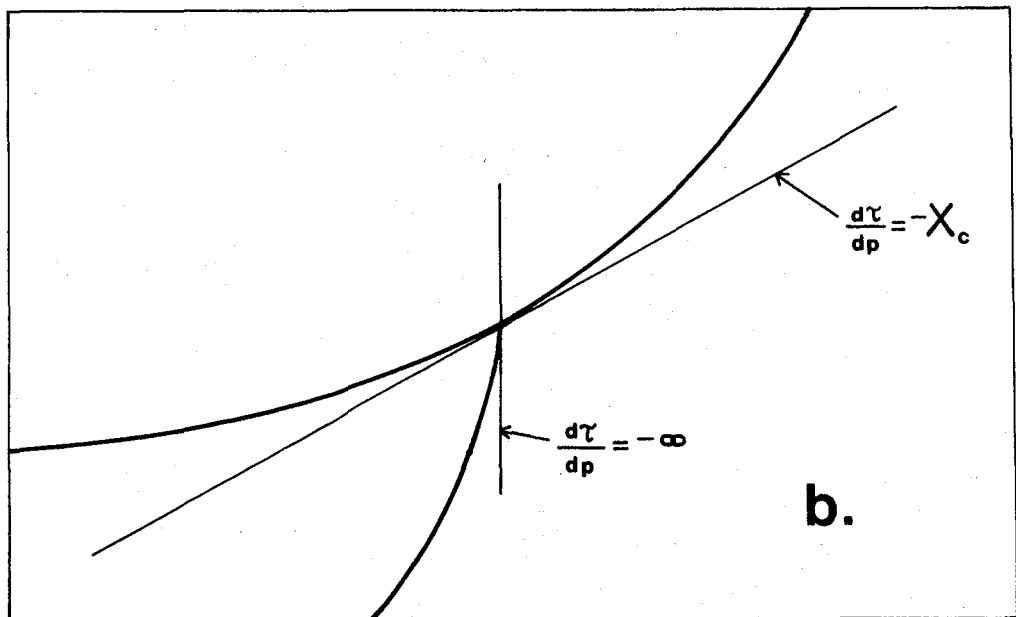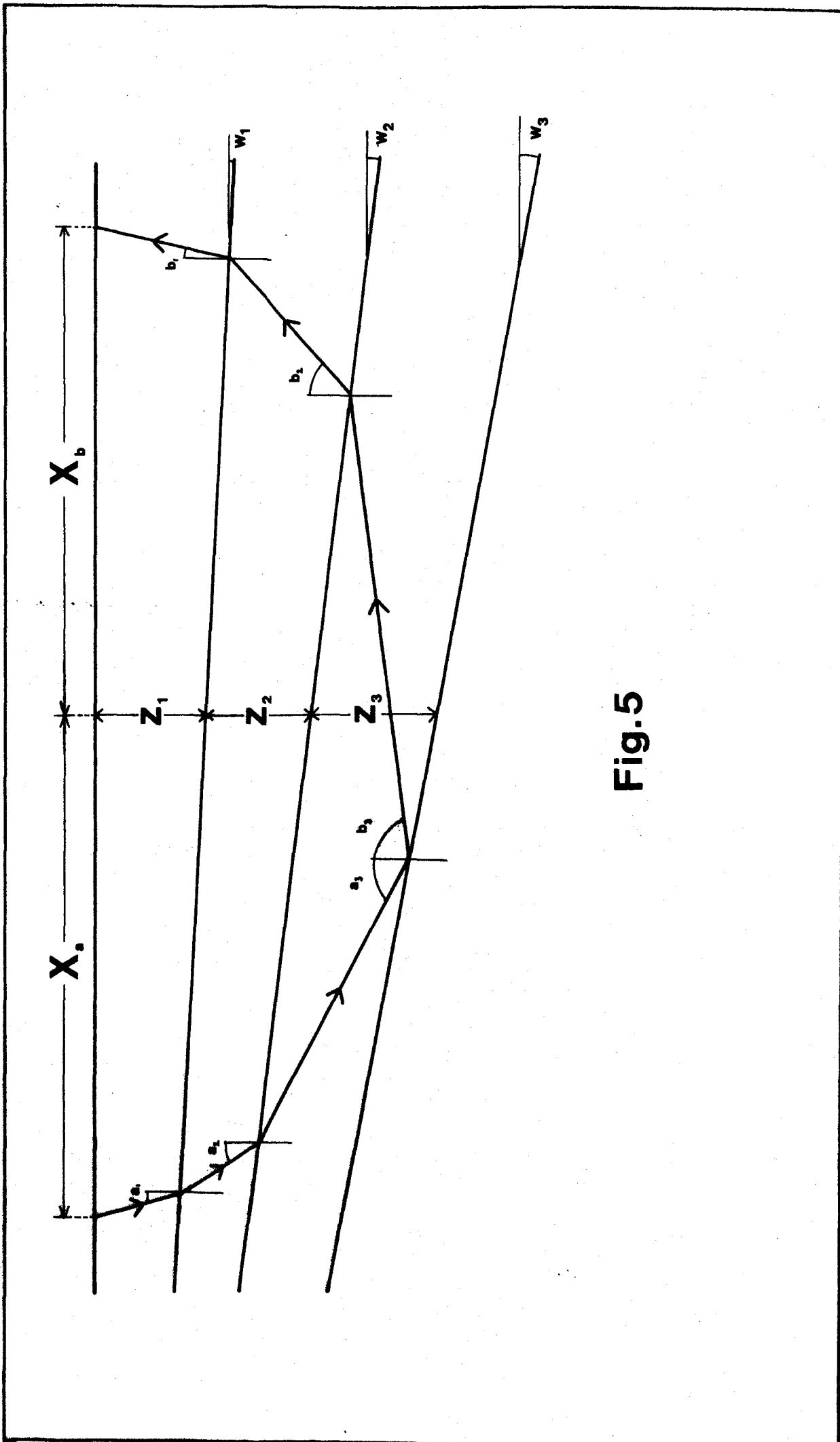
Fig.4

Fig.5

CHAPTER 3

This chapter is concerned with the method of transforming a data set in the X-T plane to that of τ-p.

3.1. Ray Parameter Stacking.

The method of Stoffa et al (1979) uses an automatic ray parameter stacking method and is employed by Bowen (1980) and Smith (pers. comm.) their computer programs to perform this transformation.

It is apparent from equation 12 for the plane, horizontal layer case that a straight line such as that from a refracted arrival in X-T is transformed to a point in τ-p and vice versa.

Ray parameter stacking involves the discrete summation of data in X-T of a C.D.P. gather by taking linear trajectories of gradient p and intercept time τ . The value at the point (p, τ) will be the sum of all X-T data that are intercepted by this trajectory. By taking many values of τ and p it is possible to obtain a complete mapping.

The process is only an approximation of the 'true' values in τ-p however, because of the finite length of the observational data in X-T and the finite sampling density. Even so, the main problem in obtaining good resolution is inherent in the linear trajectory summation process. For refracted events which occur as straight lines in X-T, there will be a large value of ray parameter stack at the single point, say (p, τ), which defines the straight line over which the event occurs. Hence, a refraction gives a clearly defined maximum amplitude point in τ-p. Reflections will occur as approximately hyperbolic events in X-T and will, therefore, map not as single points in τ-p, but as ellipses as shown previously.

Thus, in X-T, no single, linear trajectory will accurately describe the whole of a reflected wavefront, but rather a range of

different trajectories is required. It is essentially a problem of attempting to model a curve by a series of straight lines. The method of Stoffa et al (1978) relies on the assumption that it is possible to obtain a value of stack at the point corresponding to tangency that is significantly larger than the values obtained from non-tangential trajectories. The validity of this assumption depends on the curvature of the wavefront at the point of tangency, amongst other factors.

3.2. Definition of Stack

Stacking is a well-known method of signal enhancement and multiple suppression and is comprehensively described by Mayne (1962). The concept of slant stacking is suggested by Schultz and Claerbout (1978) in order to synthesize wavefronts and estimate velocities, and is applied to common shot data to transform into a p-gather which is similar to the methods employed in the programs used in this work. Henry and Orcutt (1980) describe a method of slant stacking data at a number of ranges in order to synthesize the τ-p curve.

The method of stacking assumes that there is some constant value, called the datum level, to which random noise has been added and from this assumption it follows that

Stack, $S = \dfrac{1}{M} \sum (f_i + n_i)$ where

f_i = datum level or arithmetic mean of the series

n_i = random noise

M = number of elements

Further,

$$S = \frac{1}{M} \left(\sum_i f_i + \sum_i n_i \right)$$

$$= \frac{1}{M} \sum_i f_i \qquad \text{(for random noise)}$$

$$= M \, f_i / M$$

$$\therefore S = f_i \qquad\qquad (22)$$

It is thus permissible to regard the stack as a filter passing only the mean level or D.C. component of the series. Since the D.C. level is zero for purely random noise, a separation of signal from noise is achieved.

A linear stack along a refraction will be well represented by the model described above, but a curved reflection wavefront clearly will not. This is not the only problem with the method of transformation of Stoffa et al (1979).

3.3. Aliasing

Aliasing is the most serious practical problem in the method of ray parameter stacking previously described, and is inherent in the approximate nature of the transformation. In the stacking process, significant energy may be obtained from summations along trajectories that are not tangential to any arrival in X-T but intersect the arrival non-tangentially. This effectively reduces the signal to noise ratio thus diminishing the resolution. In extreme cases, aliasing from large energy arrivals may completely overwhelm the tangential contribution from a low-energy arrival.

An example of the way that aliasing results from ray parameter stacking is shown in figure 6.

The contribution from trajectory A gives an aliased result, while the trajectory B gives the required contribution to the stack.

For a curved event in X-T, the aliased contribution will increase with the curvature of the event, and for small offset reflections, the aliased contribution may be indistinguishable from the tangential one.

For a linear event in X-T, the difference between the contribution from the tangential trajectory and an aliased contribution will be a factor of N, where N is the number of channels over which the
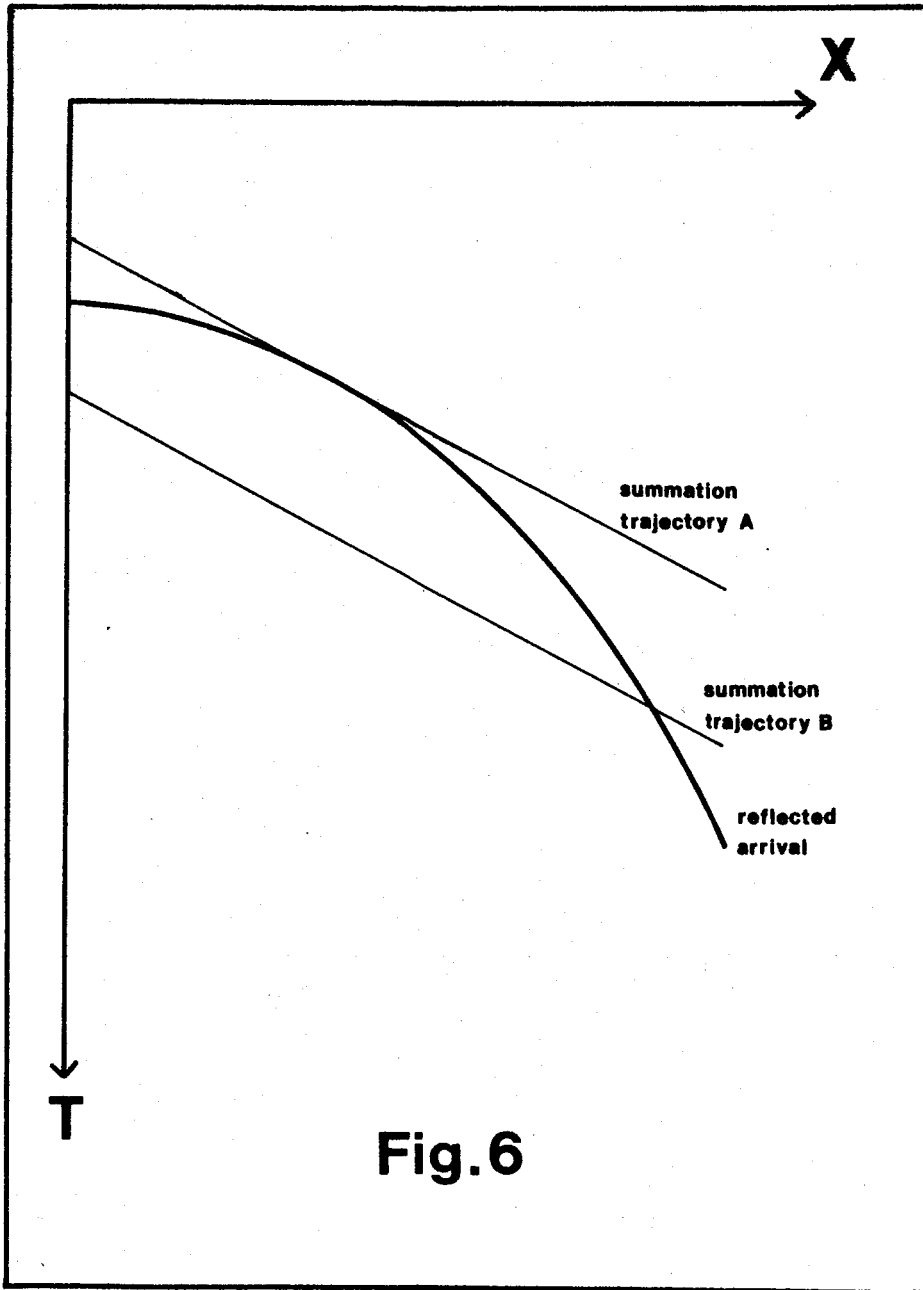
Fig.6

summation is performed, since the true tangent will 'intercept' the
event N times while the alias will only intercept once.

A typical curved event in X-T and its transform to τ-p, as
shown in figure 7, illustrates the region in which aliasing is likely
to occur (indicated by shading). This area is defined by all
trajectories that intersect the X-T curve.

Aliasing is thus seen to arise because of the approximations
involved in the actual transformation and is inherent in the method.
A way of suppressing the effects of aliasing ought therefore to be found.

3.4   Alias Suppression Using the Semblance Function

The semblance function, although originally developed for use in
velocity analysis, is nevertheless useful for the suppression of alias-
ing because of its property of emphasising coherent arrivals over
several adjacent channels with moderately low signal to noise ratios.
Tangential trajectories will show similar values and characteristics of
stack across channels whereas aliases generally appear as single high
values superposed onto the background noise. This suggests that
semblance can be used as a 'window' function which will produce unaliased
data in τ-p.

The semblance function may be defined as:

$$\text{Semblance, } K = \sum_{gate} \left(\sum_{channel} f_i \right)^2 \Big/ M \sum_{gate} \sum_{channel} f_i^2 \tag{23}$$

where the gate is the time window over which the function is calculated.

If only one sample per channel is considered, then it is straight-
forward to show that semblance may be expressed as a normalised input
to output energy ratio since

$$K = \left[\sum (f_i + n_i) \right]^2 \Big/ M \sum (f_i + n_i)^2$$

$$= M^2 f_i^2 \Big/ \left(M^2 f_i^2 + M \sum n_i^2 \right)$$

$$= 1 - \left[\left(\sum n_i^2 \right) \Big/ \left(M \sum f_i^2 + \sum n_i^2 \right) \right] \tag{24}$$

Thus the maximum value of semblance is unity, when there is no
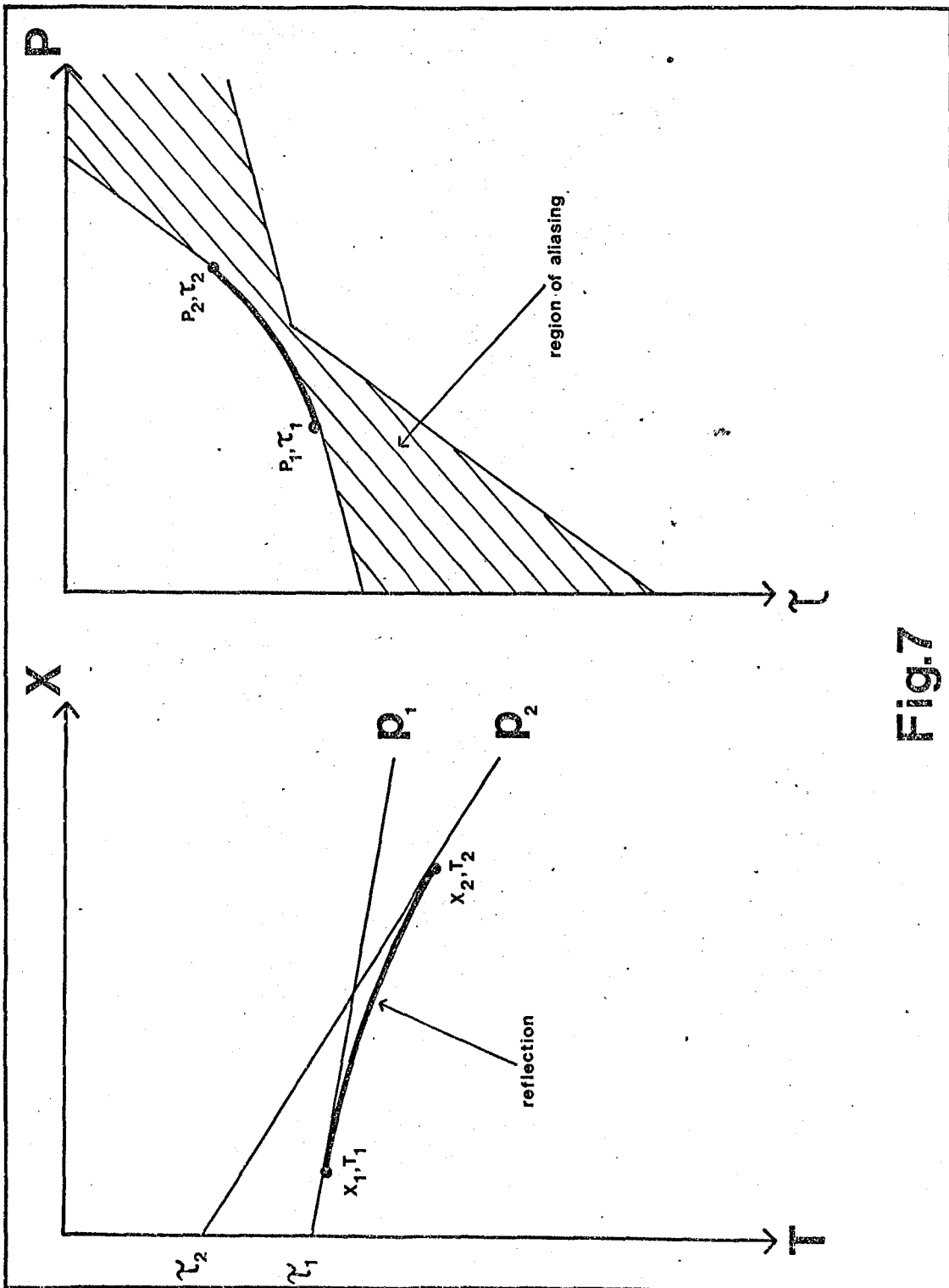noise present. When the semblance is calculated over a time gate, the

Fig.7

result is an average value over the gate-length and a high value is indicative of waveform similarity across channels.

This function is calculated over hyperbolic trajectories in the velocity analysis of reflection data, but linear trajectories are used here since values of semblance are required for particular values of ray parameter. As aliased summations tend to show less uniformity of waveform character over adjacent channels than tangential summations, the value of semblance ought to be lower for the aliased summations. It is therefore theoretically possible to discriminate against aliasing by applying a windowing filter based on some arbitrary threshold level of semblance below which all data are set to zero.

Computer programs were written by Bowen (1980) and Smith (pers.comm.) which automatically transform data from X-T into τ-p and perform semblance calculations for alias suppression. The C.D.P. data sets with which the programs were run were provided by synthetic seismograms rather than real field data. This enabled a control to be kept over the input data and meant that the results obtained for the velocity structure could be directly compared to the original model from which the synthetic data was calculated.

3.5.   Problems Associated with the Method.

Amongst the problems associated with interpretation of the τ-p diagrams are:-

(a)   The complete trajectory in the τ-p quadrant is not observed because the input data does not start at zero offset or continue to an infinite value of offset.

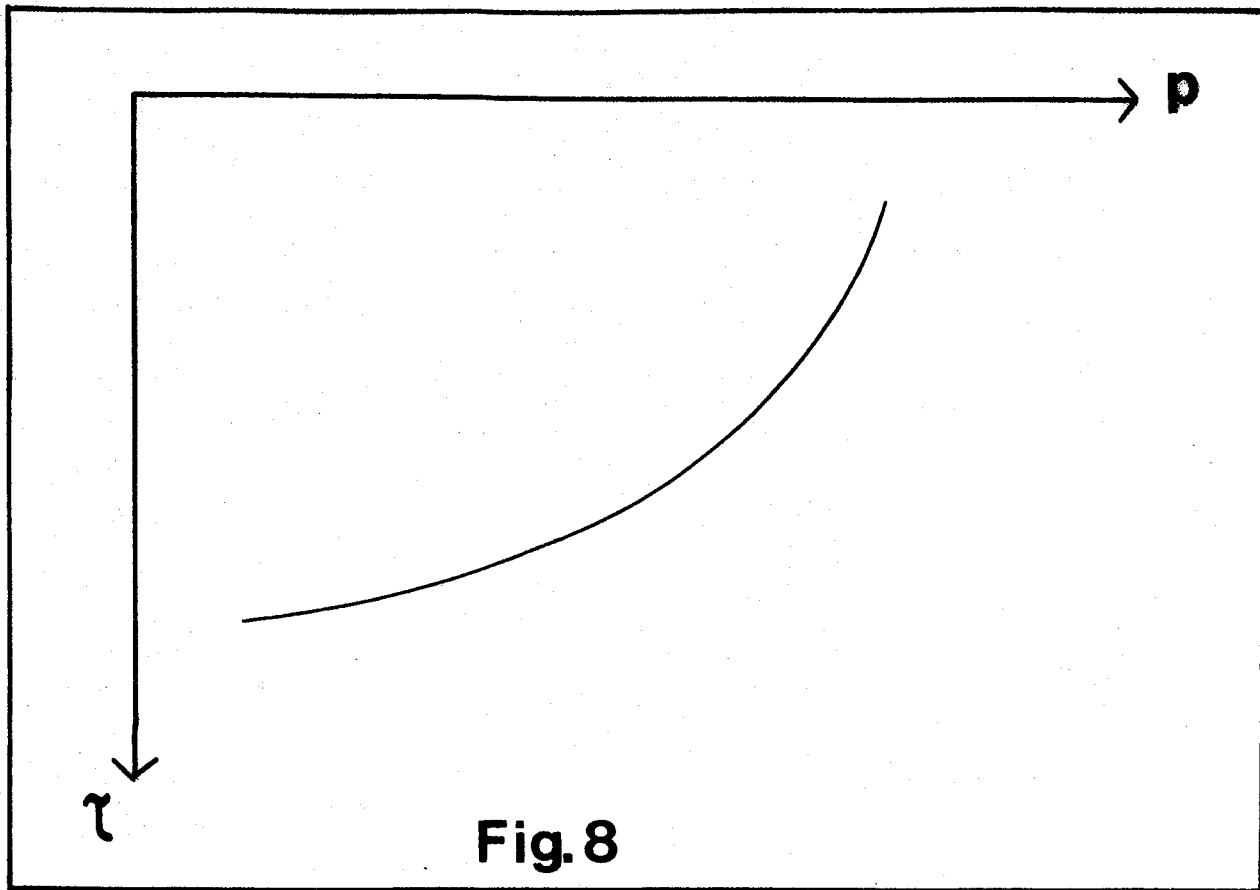A typical τ-p trajectory for a single reflector is shown in figure 8.

Fig. 8

The missing portions at either end of the trajectory correspond to zero offset where $p = 0$ and infinite offset where $p = 1/v$.

(b) The character of the waveform in τ-p varies along the trajectory. This is because at the more curved regions of the X-T trajectory (at near-offset) less of the channels are intercepted by the summation trajectory and therefore the waveform is less well defined than at large offsets where the X-T event is more linear. Also some trajectories appear not to detect the X-T event at all. This is due to the way that the data are discretely sampled.

(c) In the simple stacking program with no alias discrimination, aliasing is present even for well-defined X-T curves with relatively high signal to noise ratios. Using semblance threshold levels as a means of

windowing the data, improvements in the signal to noise ratio in τ-p
are observed, but at the expense of a decrease in resolution, particularly
at small values of p.

3.6. A Modification to the Method

The more sophisticated programs written by Bowen and Smith
utilise a method of alias discrimination originally proposed by
Schultz and Claerbout (1978).   Since it is only the tangential summations
that are required, it is clearly preferable to perform the stack calcu-
lation across the tangential channels only, ignoring the contributions
from other channels that may intercept events non-tangentially. Again
the semblance function is employed but in a different manner.   Since the
semblance should be higher along a trajectory in a region of tangency, it
ought to be possible to identify this region by calculating the semblance
for individual sections along the trajectory and then calculating the
stack for the region of highest semblance only, ignoring the rest of the
trajectory.   The method of achieving this computationally is to calculate
the values of the semblance and stack over a certain number of channels
along the trajectory (the scan or window) then step the window along to
the next position, re-calculate the functions, compare the new semblance
value with the old and retain the value of the stack corresponding to the
largest value of semblance, which will hopefully be the tangential part,
if there is one, of the trajectory.   Figure 9 shows a diagrammatical
representation of the window.

The results obtained with the modified program are considerably
improved.   There is better identification of reflected events in
X-T, less distortion of waveform character in τ-p and greater resolution.

Program outputs showing τ-p plots for synthetic data illustrate these
points and are given by Bowen (1980) and in chapter 4 of this thesis.

Listings of the programs are also given by Bowen (1980) and Smith (pers. comm.) and were written for use with the PDP11/34A/F.P.S. Array Processor Computing system owned by the Department of Geological Sciences, University of Durham.

Fig.9
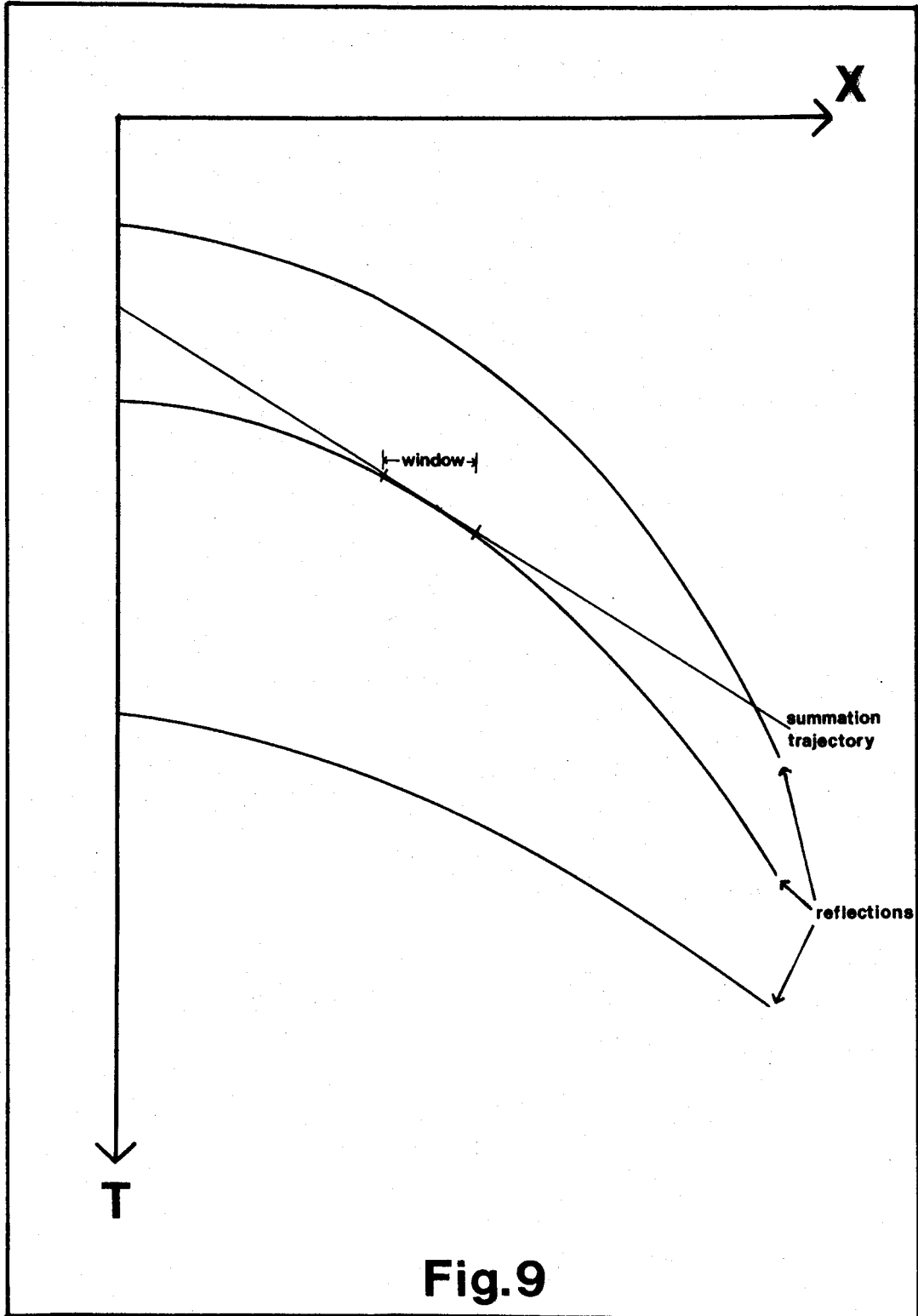
CHAPTER 4

4.1 Program Test Runs

The simple ray parameter stack programs and the modified anti-
alias programs were tested using synthetic data created by a program
(ANSEI) which produces C.D.P. gathers by calculating the normal
moveouts at selected offsets for a given stacking velocity structure,
and convolving the resultant impulse response function with a Ricker
wavelet, assuming plane, parallel, homogeneous layers. An example of
the data used is shown in figure 10, with the input parameters
indicated in figure 11.

Bowen's simple program (ABPAN) was run with this data and the
resulting output obtained is shown in figure 11, where the values
along the p-axis are in milliseconds per metre.   The predicted
ellipsoidal trajectories are visible, but so are the features of wave-
form character distortion, limited resolution at large values of p and
aliasing.   These are all to be expected because of the discrete
sampling and the finite range of offset.

Bowen's anti-alias program (ABSCAN) was then run with the same
data.   In order to reduce the running time, values of stack and
semblance at large values of τ and p were automatically zeroed.   The
result, shown in figure 12, shows increased resolution, greater wave-
form character consistency across adjacent channels and slightly
extended trajectory range.

Smith's program (MSTAUP) was run on a similar data set produced
from a three-layer model with slightly different parameters, and the
results obtained are as expected.   In figure 13, the simple program
has produced an output that suffers from all the faults of ABPAN.
In addition to the inconsistency of waveform character along the
trajectories the amplitude is also seen to vary.   Aliasing is preva-
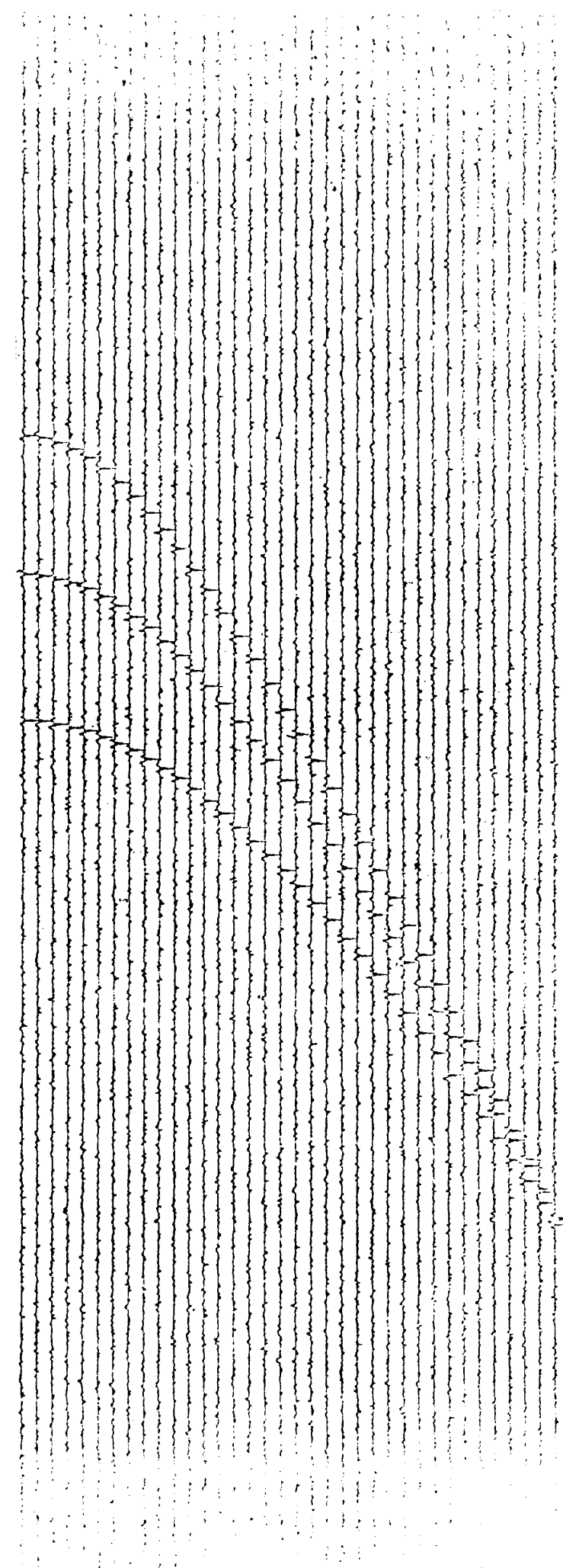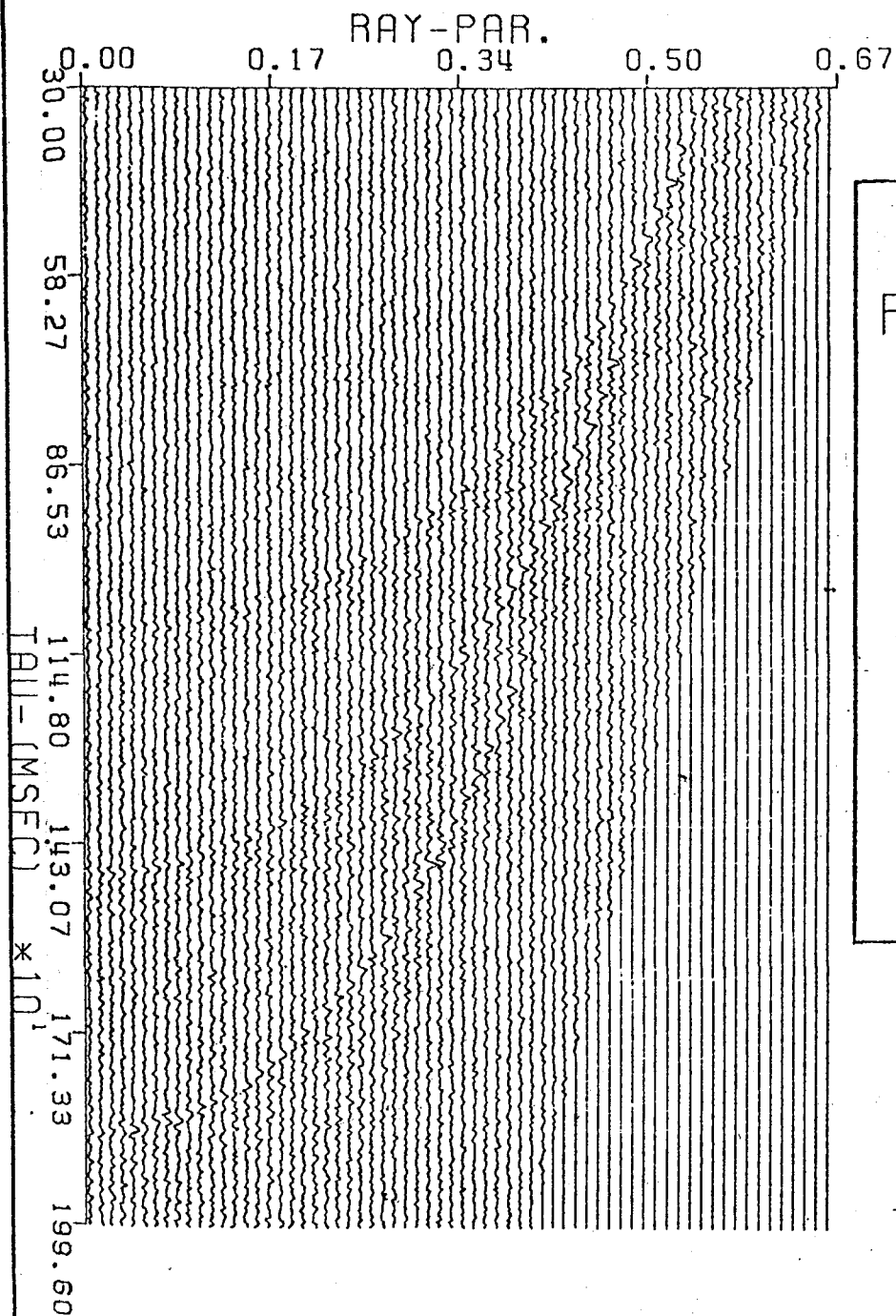lent, the individual streaks corresponding to aliased trajectories

TIME
(seconds)

Fig.10

Fig.11

RAY-PAR.

RAY PARAMETER STACK FØR
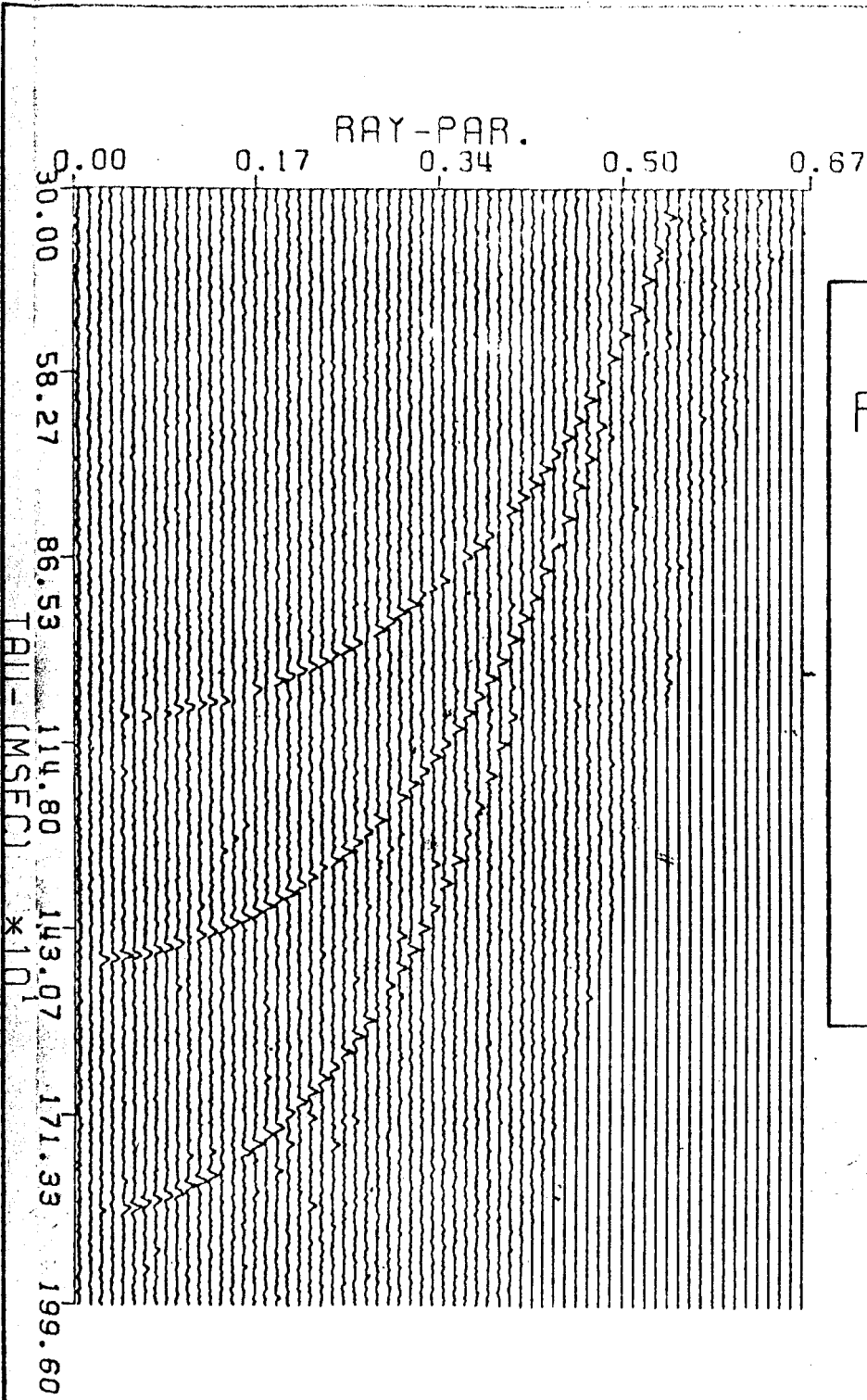
NTAU= 375

NP= 66

MODEL:

Xmin = 50m
Xstp = 150m
NCHAN = 36
S/N = 10/1

Velocity (km/s)	Thickness (km)
1·8	1·0
2·2	0·4
2·6	0·5

TEST RUN

Fig.12

RAY-PAR.

0.00   0.17   0.34   0.50   0.67

TAU-(MSEC) *10¹

30.00   58.27   86.53   114.80   143.07   171.33   199.60

RAY PARAMETER

STACK FOR

NTAU= 375

NP= 66

MODEL AS IN FIG.11

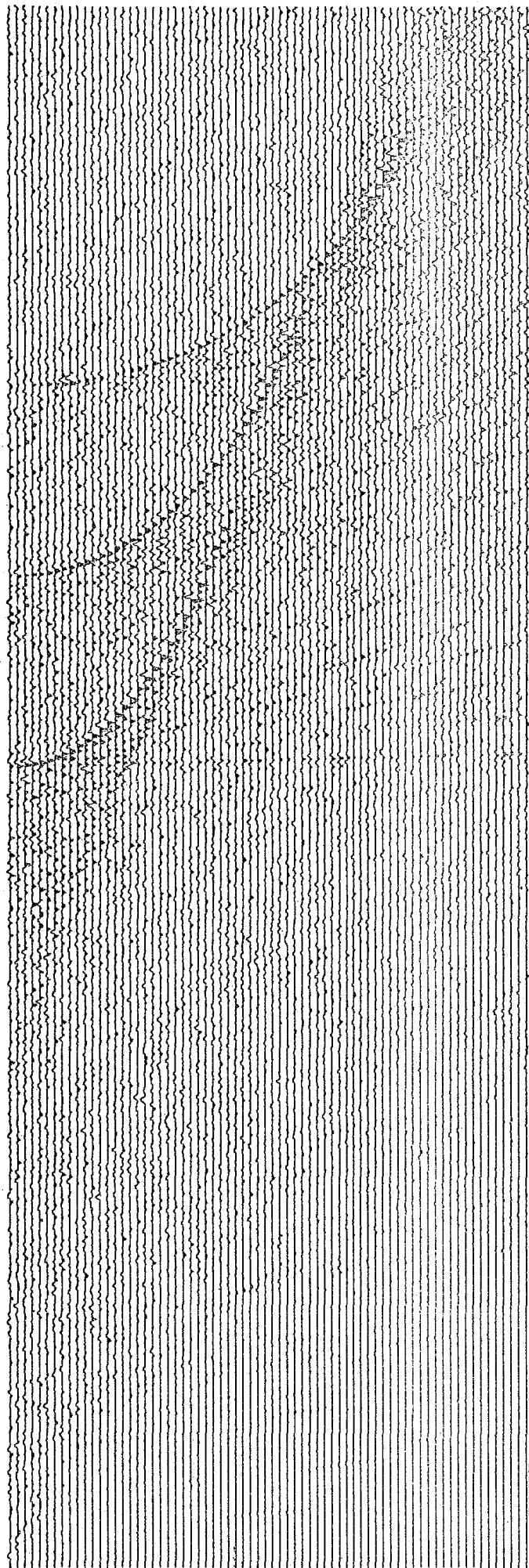ANTI-ALIAS
PARAMETERS:

SCAN:
3 CHANNELS

STEP SIZE:
1 CHANNELS

TEST RUN

RAY PARAMETER
(ms/m)

0   0·69

TAU
(seconds)

0

1

2

3

4

Fig .13

NTAU = 70

NP   = 1024

MODEL:

Xmin   = 50m
Xstp   = 150m
NCHAN = 36
S/N   = 10/1

Velocity (km/s)	Thickness (km)
1·8	0·90
2·6	0·75
3·6	0·95

being visible, particularly for the lower ellipse where it intersects the τ-axis. This form of aliasing is partly due to the truncation of the data and is termed the 'end-effect' by Schultz and Claerbout (1978). It may be suppressed by extrapolation of the data beyond the axis, as well as by the methods already discussed.

Figure 14 shows the result of running Smith's anti-alias program with the same data. The increase in resolution and particularly in signal to noise ratio is just as dramatic as with Bowen's programs, although the consistency of waveform character leaves room for improvement with both anti-alias programs. The limited extent of the τ-p trajectories, particularly at large values of p, is due to the small range of offset used in the model data set.

The two anti-alias programs are similar in the way that they perform the transformation and so the similar results are to be expected. Smith's program has, however, a significantly smaller average running time which makes it more practical. The program was completed in August, 1982, by which time all of the data processing had been completed. Therefore, all of the τ-p plots shown in Chapter 5 are produced from either Smith's simple program, or from Bowen's programs.

4.2. Interpretation of the Tau-p Trajectories

Interpretation of the obtained results was attempted and the limited range of the τ-p trajectories was found to be a problem. The ellipses are difficult to follow at small values of τ and this is the region of the trajectory where the velocity information is directly obtained (see figure 4). None of the obtained plots clearly show the upper ellipse actually intersecting the p-axis to give the horizontal slowness of the upper layer, and neither the second nor third ellipses are clearly seen to intercept the ellipse above them. It requires extrapolation by eye, with the knowledge that the trajectory becomes asymptotic to the normal at the point of intersection, to estimate the correct value of p. This
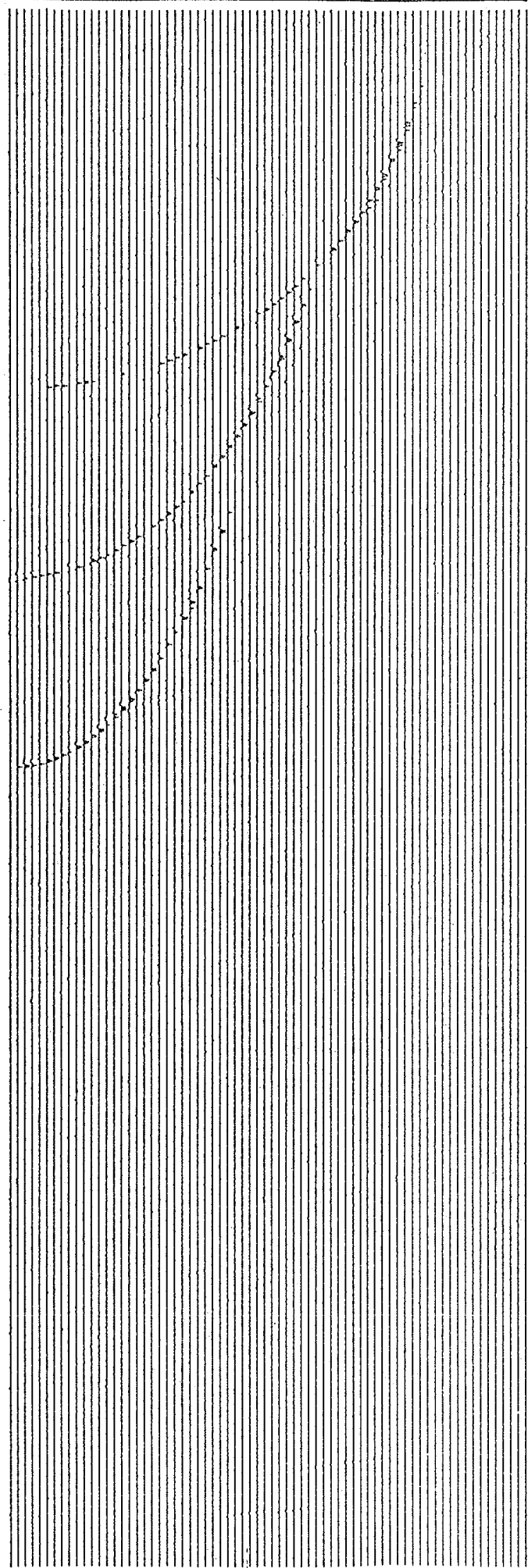
Fig.14

RAY PARAMETER
(ms/m)

TAU
(seconds)

NTAU = 70

NP = 1024

MODEL:

Xmin = 50m
Xstp = 150m
NCHAN = 36
S/N = 10/1

Velocity (km/s)	Thickness (km)
1·8	0·90
2·6	0·75
3·6	0·95

problem is simply due to the fact that the X-T data do   not extend
to an i:finite offset.

    If the data have a particularly small range of offset then the
extent of the τ-p trajectory may ·be so limited, such as in figure 15,
that it may be difficult to accurately deduce the velocity structure
by merely extrapolating the trajectory by eye.

Fig.15
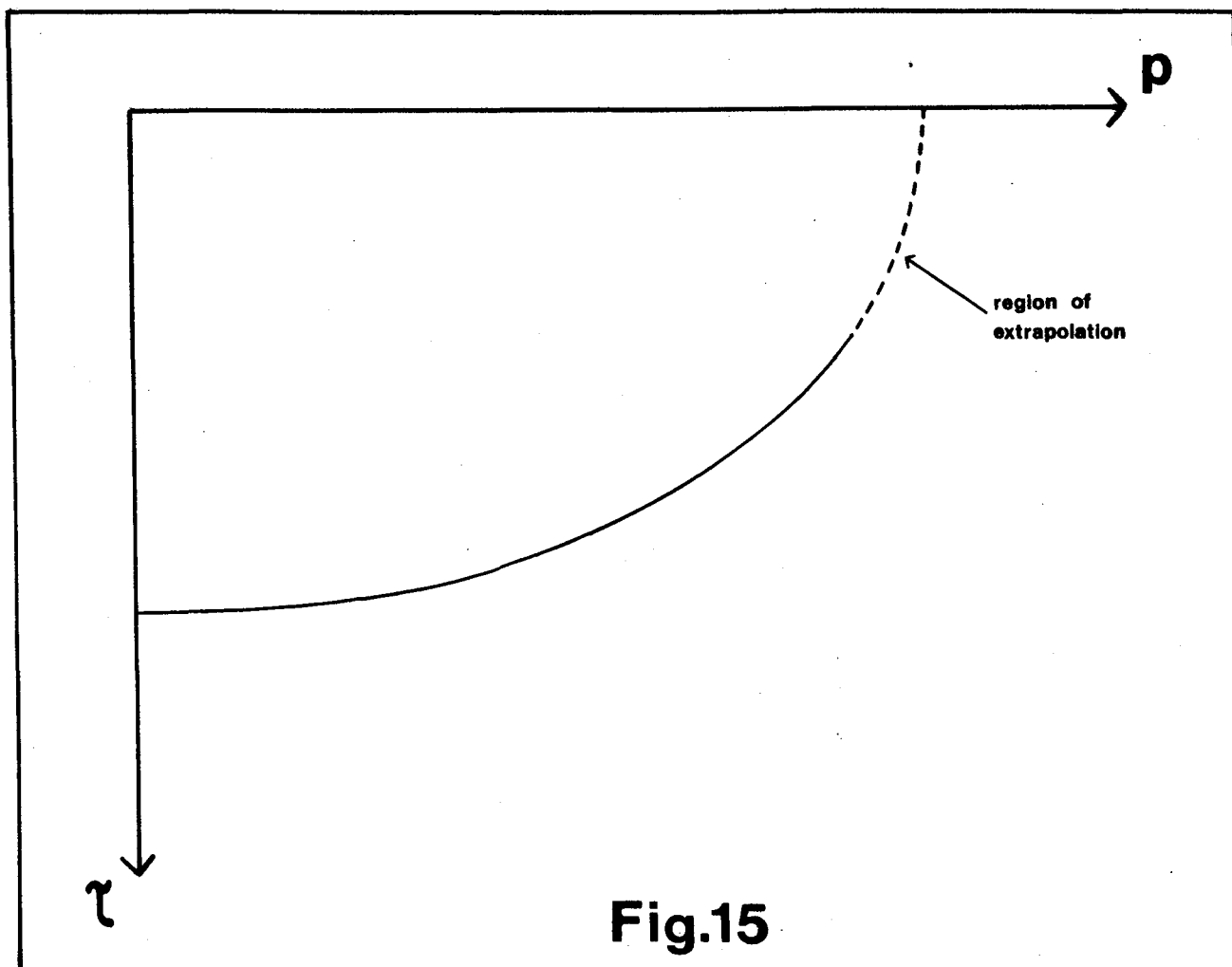
    In this situation it may be necessary to assume that the
trajectory is a true ellipse and then attempt to model it with a set of
different elli~ses until a goo:' fit is found. A'ternatively it is

possible to obtain a unique solution to the required ellipse knowing
only two points that lie on it. This is apparent from the general
equation of an ellipse:

$$\frac{x^2}{a^2} + \frac{y^2}{b^2} = 1 \qquad\qquad (25)$$
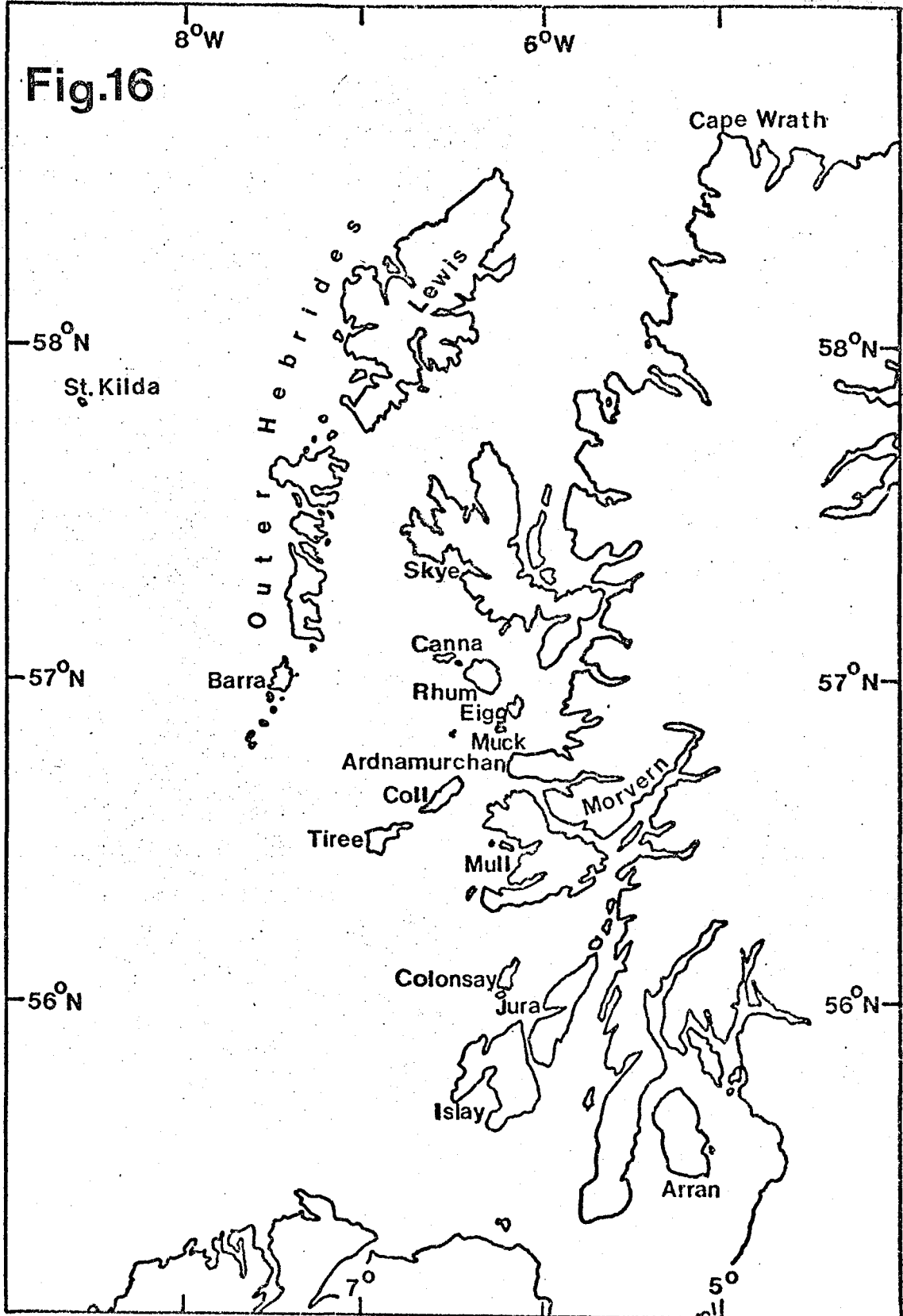
, where

a = intercept on the x-axis and

b = intercept on the y-axis

Since there are only two unknowns, a and b, in the equation, any
two points on the ellipse will uniquely define it.

The measure of accuracy of this method depends on the validity of the
assumption that the τ-p trajectory is well represented by a true ellipse,
and this may be difficult to assess accurately without direct knowledge
of the velocity structure.

The approximations that are inherent in the transformation process
which have been discussed arise from the method of modelling a curved
event in X-T by a series of linear trajectories. The further problems
of aliasing, loss of resolution, distortion and limited trajectory range
have all been considered. The major problem in estimating the velocity
structure using synthetic data is the one of limited trajectory range but,
as will be seen, the other limitations of the method may become more
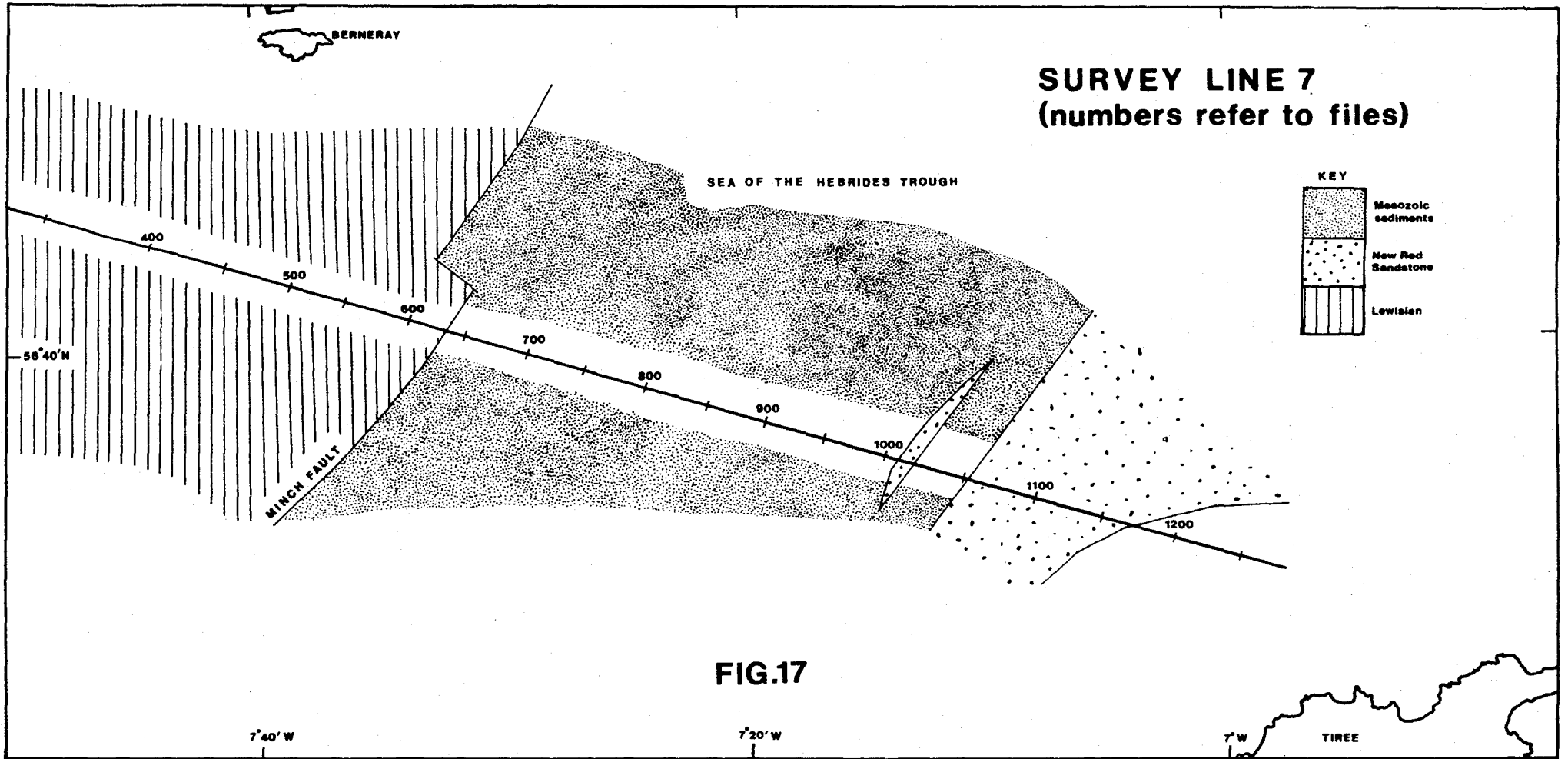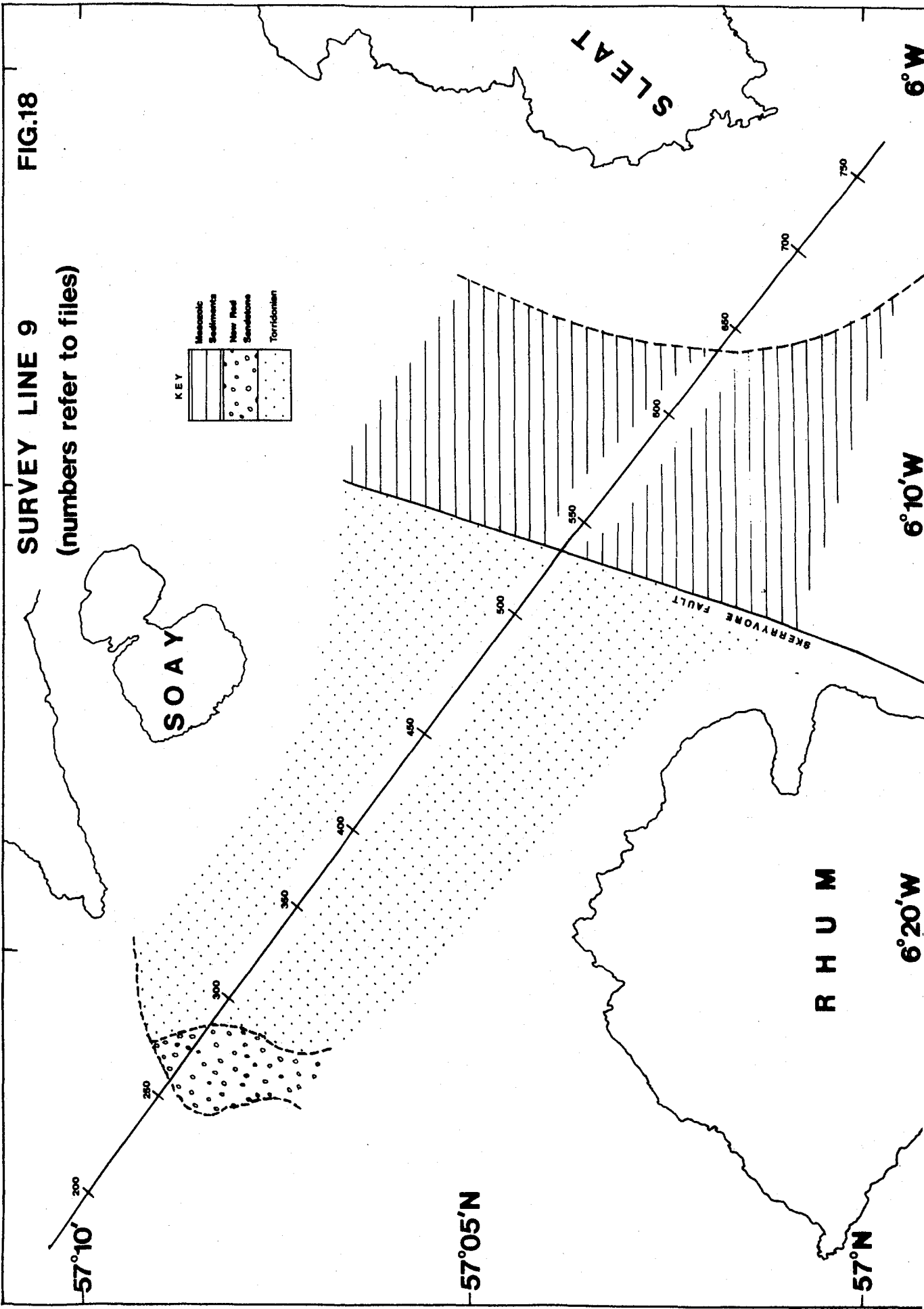apparent when using real data.

Fig.16

SURVEY LINE 7
(numbers refer to files)

BERNERAY

SEA OF THE HEBRIDES TROUGH

KEY

Mesozoic
sediments

New Red
Sandstone

Lewisian

400

500

600

700

800

900

1000

1100

1200

56°40'N

MINCH FAULT

FIG.17

7°40'W

7°20'W

7°W

TIREE

FIG.18

SURVEY LINE 9
(numbers refer to files)

CHAPTER 5

5.1.   Processing Procedure

The survey lines from which data are taken are shown in detail in

figures 17 and 18, where the numbers marked on the lines refer to the

magnetic tape file number on which the C.D.P. gathers were recorded.   The

raw field data which were recorded in the form of twenty-four channel

common shotpoint gathers, were demultiplexed and sorted to obtain the

required twenty-four fold C.D.P. gathers.   With the data in this form it

was decided to use only the first four seconds of record as only the near-

surface geological features were of interest.   An example of a typical

C.D.P. gather is shown in figure 21.   The initial offset is 245 metres

and the hydrophone spacing is 100 metres.

The data were then processed in order to increase the signal to

noise ratio.   The processes were performed in the following order:

(a) Bandpass filtering. High frequency noise was evident on the traces,

so a bandpass filter with a cosine bell taper of width 10 Hz was applied.

This filter passed frequencies within the range 20 - 50 Hz without

attenuation.

(b) Trace edit. Some channels in the recording equipment were faulty

and large glitches, or peaks, along the trace due to amplifier switching

faults were found to completely obscure the required signal. Those

channels were zeroed.

(c) Polarity reversal. During the connecting of the hydrophones, some

instruments were connected with their polarities reversed with respect

to the others.   This is corrected by applying a polarity reversal down

the length of the trace.   In practice it was found necessary to reverse

four channels for line 7 and five channels for line 9.

(d)   Normalisation of each trace to unit amplitude enabling arrivals
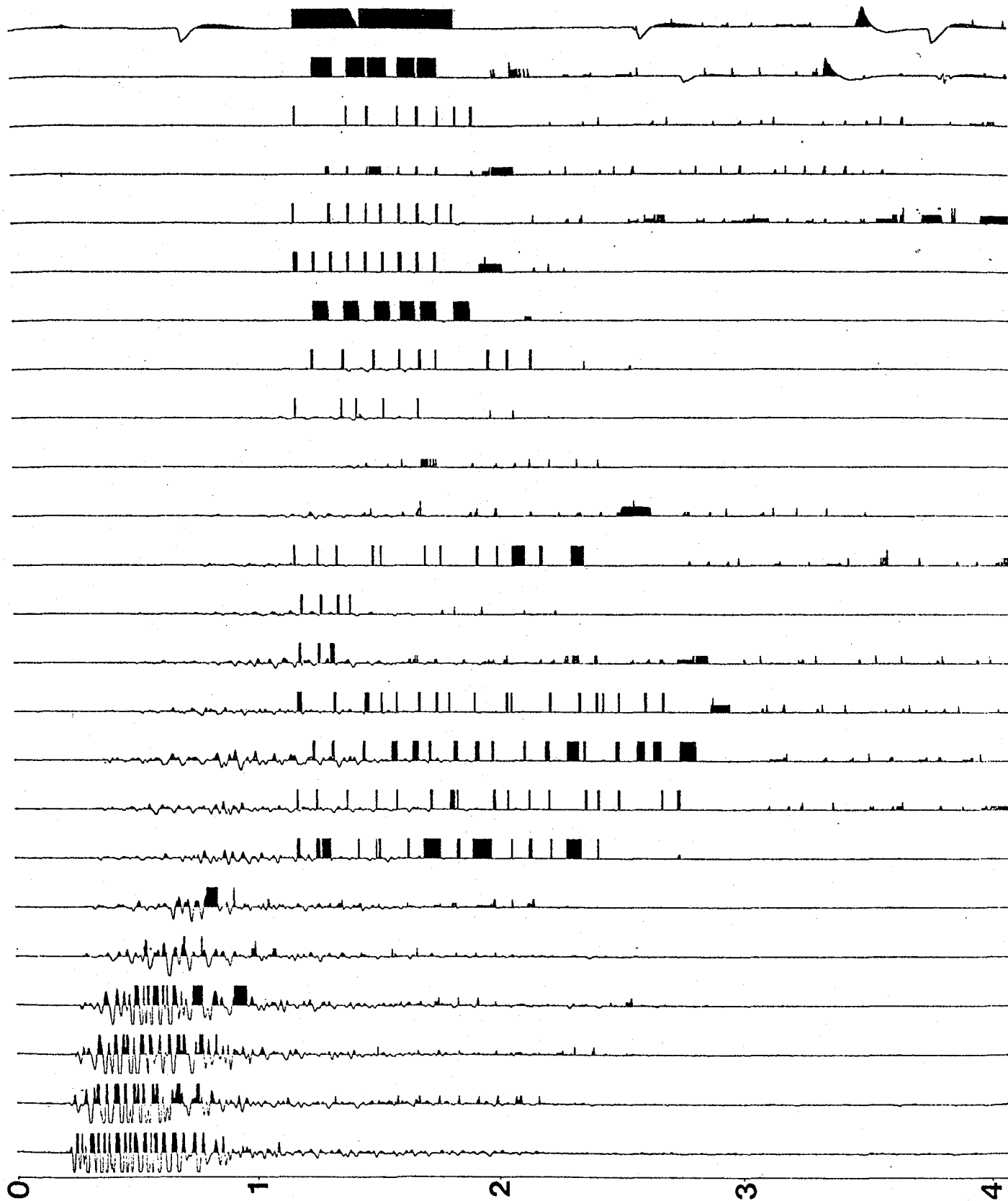
to be directly comparable across the gather.

FIG.19

The general poor quality of the data is readily seen from the unprocessed C.D.P. gather shown in figure 19. Of the 42 files on which the τ-p programs were run, only 17 were of sufficient quality to be interpreted and are shown in table 1. On average, at least two or three channels from every gather had to be zeroed due to glitches. A less extreme example of a glitch is shown on channel 17 in figure 22, which is one of the best quality gathers. For comparison, figure 21 shows the same gather before processing. The noise is particularly evident on the furthest channels and tends to mask the data, even when the bandpass filtering has been applied. Generally, it is of high frequency and hence appears as an approximately constant high frequency signal. Similarly, the more extreme cases of glitching where whole portions of traces up to about one quarter of a second long are swamped by a continuous signal, result in a constant frequency signal after the bandpass filtering has been applied. How extensive this amplifier fault is, and its effect on the data is shown in figure 19 which is an example of the quality of the majority of data. In most cases, the only arrival to be seen clearly and that could be followed along the channels was the first refracted arrival.

5.2. Interpretation

When interpreting refracted arrivals, the effect of dip should be taken into account. For the case of a uniformly dipping bed as shown in figure 20, the observed (or apparent) velocity may be corrected to give a true value.

$$\text{Traveltime of ray } S_1 R_1 = t_{s_1} + t_{R_1} + \frac{X\cos\emptyset}{V_1} \quad \text{and}$$

$$\text{Traveltime of ray } S_2 R_2 = t_{s_2} + t_{R_2} + \frac{(X+d)\cos\emptyset}{V_1} \quad ,$$

where t_{s_1}, t_{R_1}, t_{s_2} and t_{R_2} are the delay times below the indicated points to the refracting boundary.

Line 7 File 487
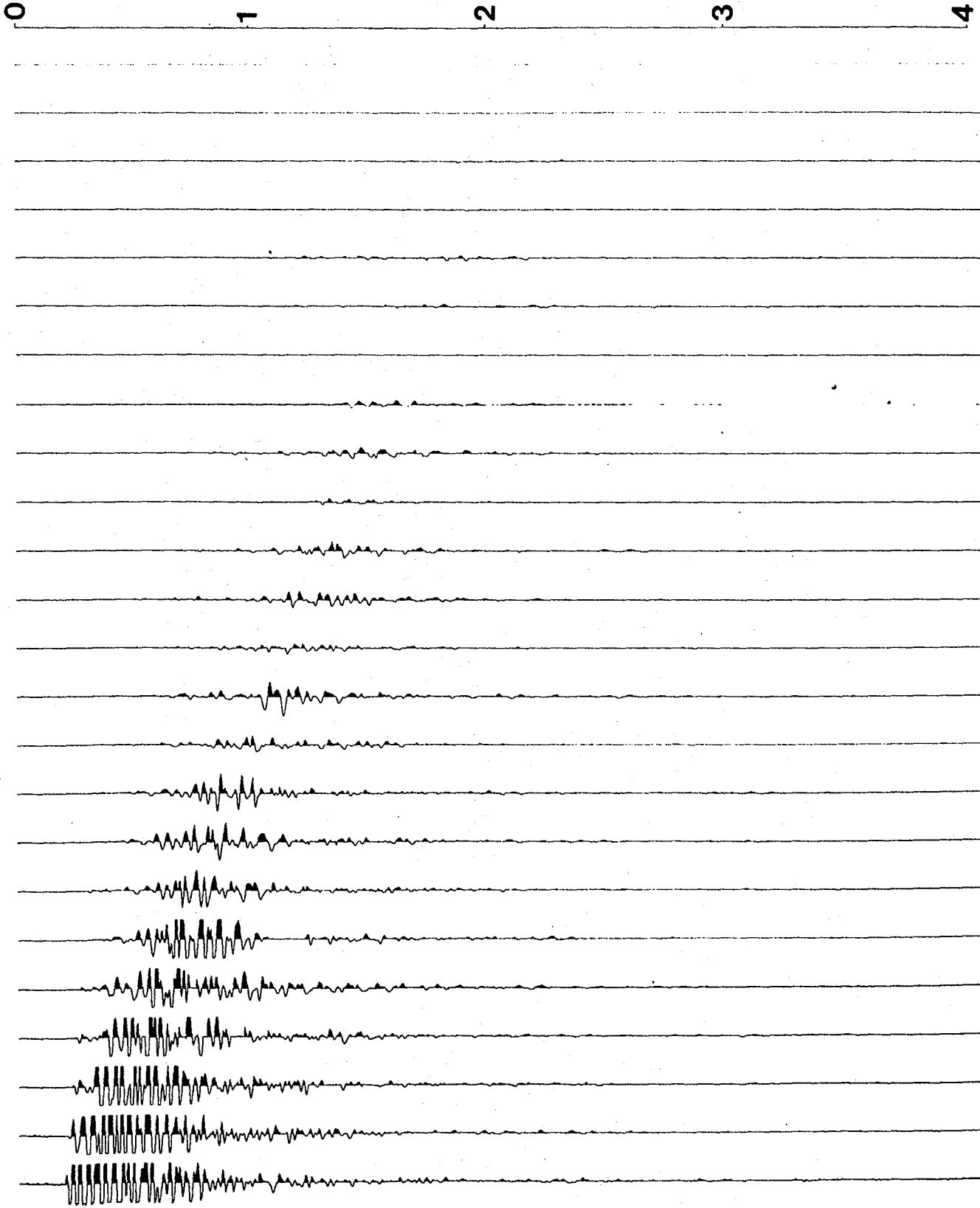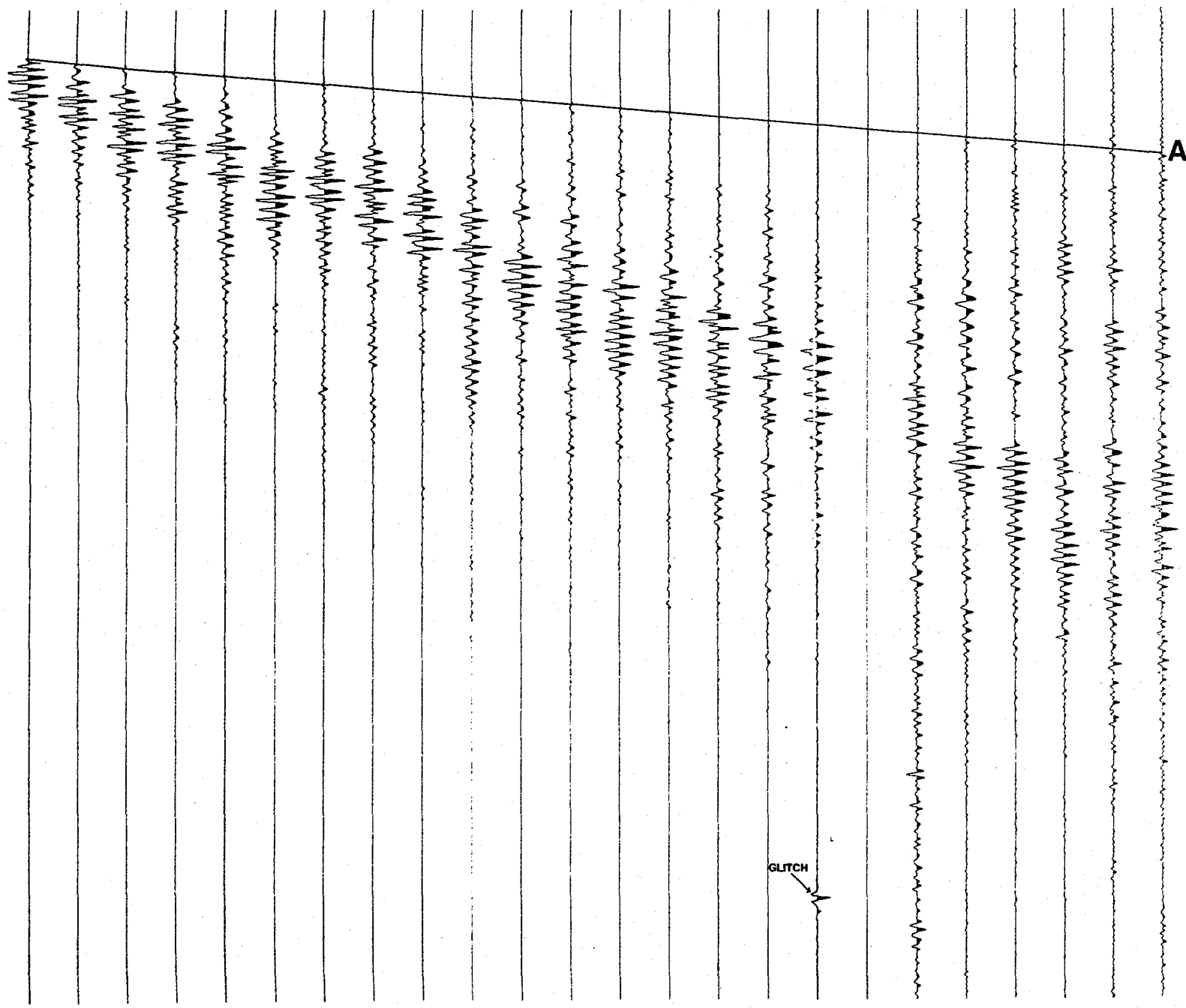Before Processing
(channel 18 edited)

TIME

0

1

2

3

4

FIG.21

Line 7 . File 487

After Processing

Parameters used:

1. UNIT AMPLITUDE NORMALISATION

2. POLARITY REVERSAL: 1, 2, 5, 10, 12, 20

3. BANDPASS FILTERING: 20-50 Hz
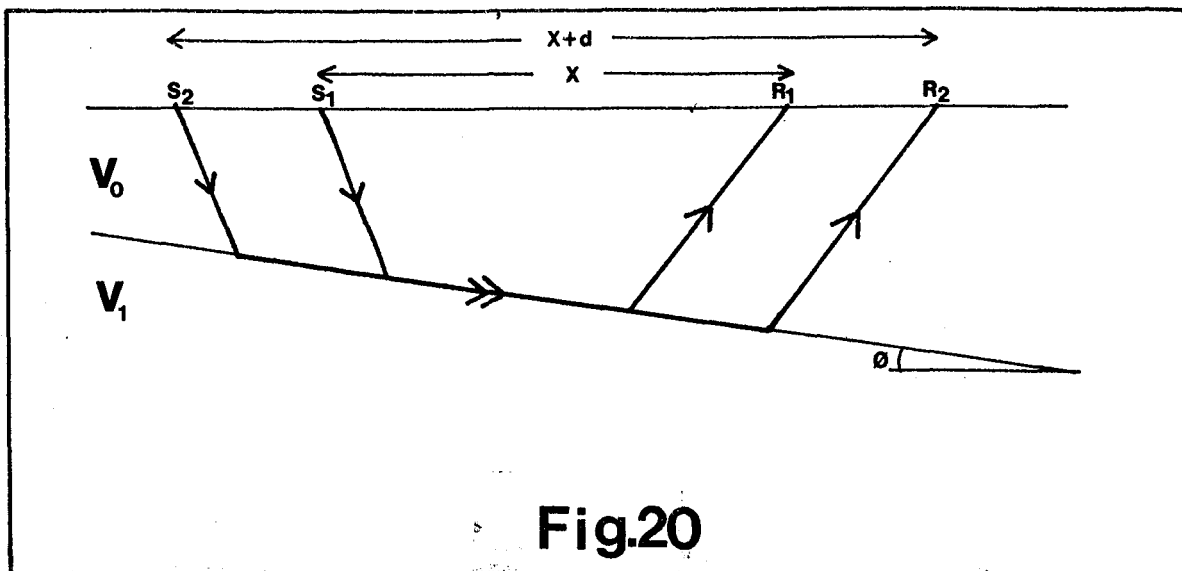
Velocity of A = 5·6 km/
(assuming no dip)

GLITCH

FIG.22

Fig.20

The apparent velocity V_1' is given by

$$V_1' = d / (t_{S_2} + t_{R_2} + \frac{(X+d)\cos\emptyset}{V_1} - t_{S_1} - t_{R_1} - \frac{X\cos\emptyset}{V_1})$$

But it may readily be shown that

$$t_{S_1} + t_{R_1} = t_{S_2} + t_{R_2}$$

Therefore,

$$V_1' = \frac{d}{d\cos\emptyset/V_1}$$

$$= V_1/\cos\emptyset \qquad (27)$$

This derivation is still valid if the source and receiver positions are interchanged.

So, for a dip of 8°, the apparent velocity is 1.11 times the actual value. For dips of less than 8° the correction will be negligible and for the data in tables 1 and 2 no corrections are needed.

5.3.   Results

5.3.1.   Line 7

The data were processed from file 352 onwards as the first few hundred files were recorded while the ship was changing direction, and

a velocity analysis was performed on every fifteenth file.

From the file 352 to file 607, the basement is Lewisian and the first refracted arrivals are seen on the C.D.P. gathers. Further down the time axis, the traces are very noisy, especially those at large offset, and result in very noisy τ-p plots, examples of which are shown in figures 23 and 24. As it is the furthest channels which are the major contributors of noise, it was decided to zero all of them from an arbitrarily chosen channel, in this case channel 12, onwards and to re-calculate the τ-p plot to see if any improvement was made. However, the fact that the total offset was so severely reduced meant that any elliptical trajectory present would have been reduced in extent, and also the random noise did not cancel out to the same degree as it would have done had the full twenty-four channels been present. Overall there was no significant improvement and it was decided to retain the full twenty-four channels, even though the τ-p plots showed no well-defined, elliptical trajectories. Even the point of local maximum stack that corresponds to the refracted arrival through the Lewisian is not apparent. This is hardly surprising when the amplitude of this arrival is compared with the amplitude of the other reflected arrivals or the noise. Since the rock is very hard and dense relative to the overlying water layer, most of the seismic energy is reflected from the sea floor rather than transmitted through it.

The value of semblance in the τ-p plane was plotted (figure 25). The data are contoured, which seems to show the maxima rather more clearly. It would perhaps have been preferable if a program had been written to present the value of stack in the τ-p plane in contoured form, but in view of the time available this was considered impractical. The values of semblance in τ-p should theoretically resemble the elliptical trajectories of stack.

ray parameter [ms/m]

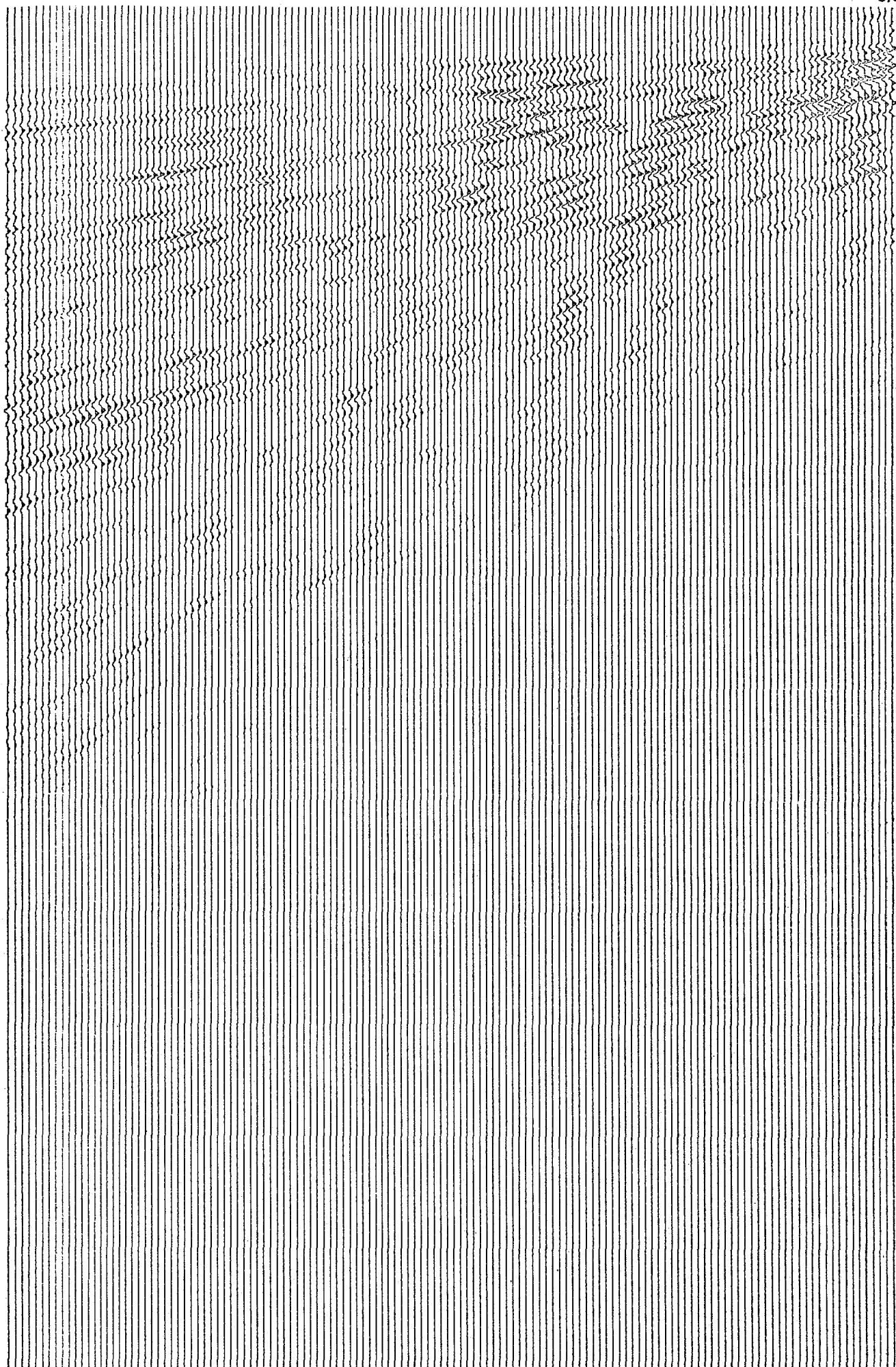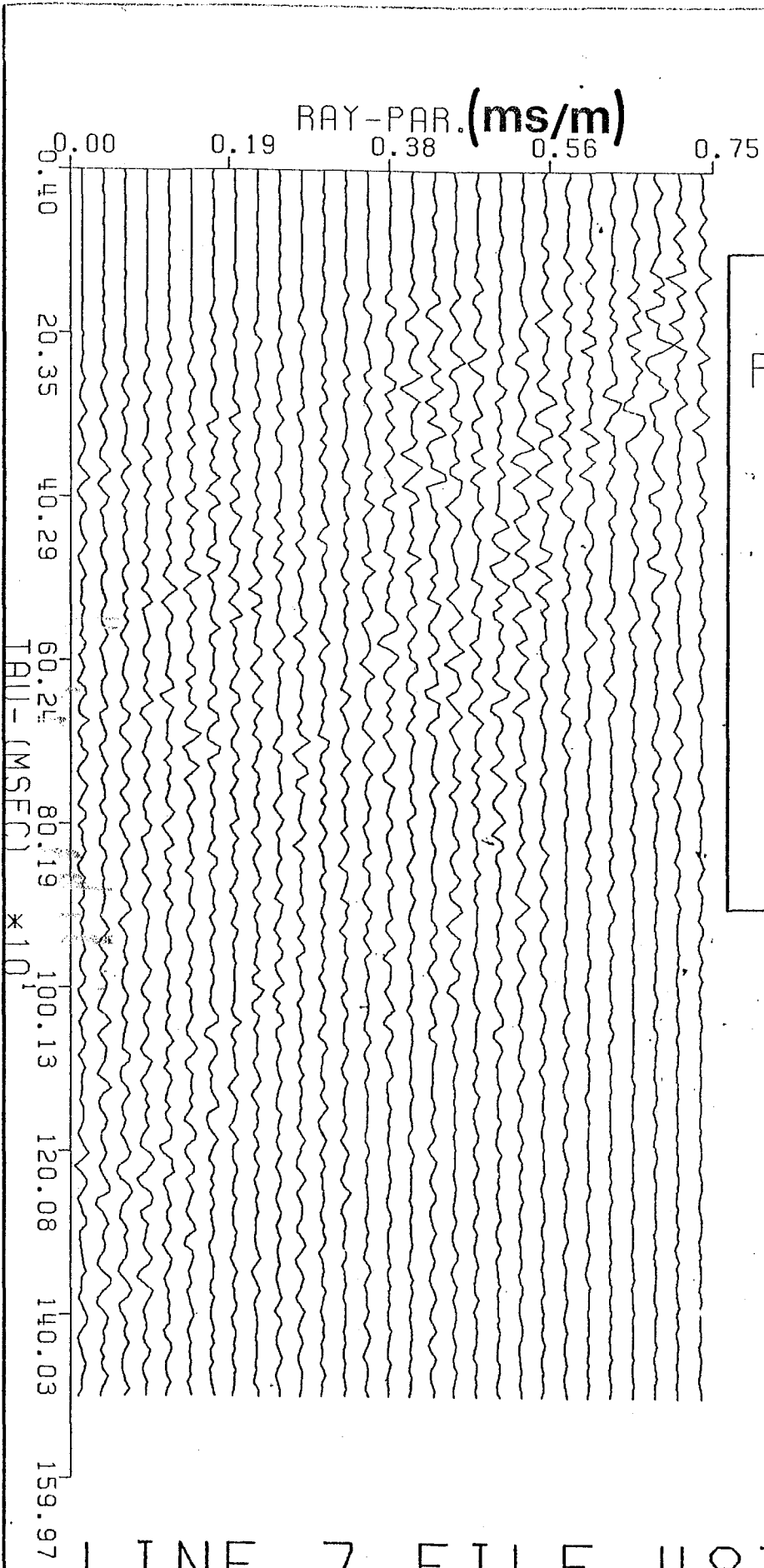0   0.67

FIG.24

RAY-PAR. **(ms/m)**

0.00   0.19   0.38   0.56   0.75

TAU- (MSEC) *10¹

RAY PARAMETER
STACK FOR
NTAU= 188
NP= 29

LINE 7 FILE 487

TAU-P SEMBLANCE CONTOURS   p[ms/m]

t [sec]

FIG.25

PROCESSING PARAMETERS

NO. OF CHANNELS = 24
SAMPLES PER CHANNEL = 1024
SAMPLE DELAY = 0
LEVEL OF INTERPOLATION = 1
CHANNEL 1 OFFSET = 245.0
CHANNEL SPACING = 100.0
SAMPLING INTERVAL MS = 4
START OF ANALYSIS MS = 4
END OF ANALYSIS MS = 1500
TIME STEP MS = 8
OPERATOR GATEWIDTH MS =8
START RAY PAR. S/KM = 0.00
END RAY PAR. S/KM = 0.70
RAY PAR. STEP S/KM = 0.03
MIN. CONTOUR VALUE = 0.10
CONTOUR INTERVAL = 0.05
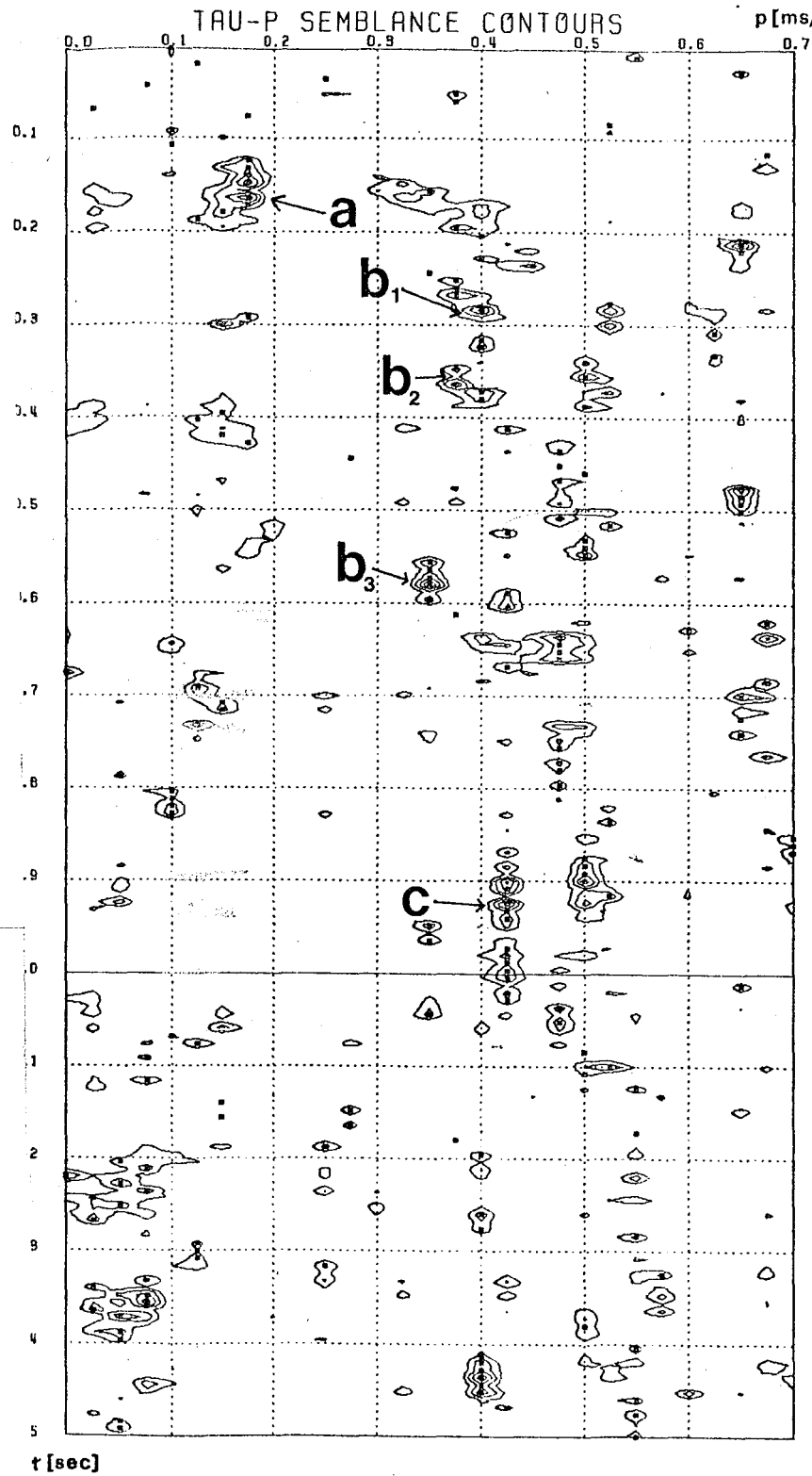
Although the elliptical trajectories are not apparent it is
possible to see local maxima..In figure 25 the maximum (a)
probably corresponds to a refracted wave.The maxima directly
below it with identical p-values are either multiple
arrivals or spurious effects due to noise.In most cases the
pulse will be extended in the τ-direction due to the nature
of the source and the proximity of both the source and the
detector to the water surface which may cause unwanted re-
flections..This leads to ambiguity in the τ-value chosen to
represent the event and results in an error of ± 0.05 milli-
seconds in τ.The beginning of the pulse (its smallest τ-
value) is taken for simplicity and consistency,although
taking the centre of the event may also be justified since
the discrete sampling density of the data , random noise
and correlation with the original X-T data are all factors
which may affect the final choice of τ-value.

For the first arrival marked on figure 25, the corresponding wave
has a velocity given by the inverse of its   p-value (1·73 milli-
seconds per metre) which is 5·8 km/s.   This value assumes that the
refracting layer is a plane, horizontal layer.   The average value
of dip was calculated for this gather and found to be less than $0 \cdot 2^{\circ}$
which did not significantly affect the final result.   This value
agrees with the calculated velocity of the first arrival marked A
on the C.D.P gather in figure 22 to within the limits of accuracy of
the results.   The value of dip for the file from which figure 22 is
taken is also negligible.   Since this arrival is the first to be
seen on the gather (the water wave is considerably slower) the measured
velocity corresponds to the velocity of the Lewisian basement.   From
the calculations performed on all of the good quality C.D.P gathers
and τ-p semblance plots up to file 607, the velocity of the Lewisian

appears to lie within the range of 5·1 to 5·8 km/s (see table 1). Using

the table of velocities for different rock types within the Lewisian

complex given by Hall and Al-Haddad (1976), the Lewisian in this area

appears to have a mainly quartzo-feldspathic composition with the possible

addition of some pegmatites and amphibolites.   The value of 4·4 $\pm$ 0.3

km/s   calculated from file 517 should also be noted.   It was not used

to calculate the average velocity of the Lewisian quoted in table 1.

This is justifiable on both statistical and geological grounds, although

it is impossible to interpret this one result as definitely representing

an isolated area of lava, even though they appear to exist in the area.

The errors quoted in table 1 arise from :-

   i) the error in the calculated velocity of sea-water.
      The values calculated from the few X-T and τ-p
      semblance plots on which the event representing
      the direct water wave was visible were within a
      range of 0.2 km/s. This is because of the diffi-
      culty of distinguishing the event from noise.

   ii) errors in the velocities calculated from the X-T
      and τ-p plots due to the difficulty of disting-
      uishing the events , undulations in the sea-bottom
      which give rise to changes in τ (these errors are
      small since the events appear to be generally well-
      aligned in X-T) , errors in the measurement of dip
      angle (this is also of minor importance as the
      error in the calculated dip is negligible ($\pm$ 0.4°)
      and the actual value was small enough to ignore any
      dip correction) and inaccuracies or inconsistencies
      in the experimental arrangement due to speed or
      direction changes of the boat.

      Second arrivals due to reflected waves from within

the Lewisian were not seen , verifying the observations

of Binns et al (1974).

TABLE 1

FILE	VELOCITY±S.E. OF FIRST ARRIVAL(km/s)	OBTAINED FROM:	AVERAGE VELOCITY (km/s)	S.D. (km/s)	ROCK TYPE
337	5.8 ± 0.4	SEMB.			
352	5.1 ± 0.4	C.D.P.			
397	5.5 ± 0.4	C.D.P.			
412	5.7 ± 0.4	C.D.P.			
442	5.4 ± 0.4	C.D.P.			
457	5.2 ± 0.4	C.D.P.	5.5	0.28	LEWISIAN
517	4.4 ± 0.4	C.D.P.			-LAVA?
547	5.8 ± 0.4	SEMB.			
577	5.5 ± 0.4	C.D.P.			
607	5.1 ± 0.4	BOTH			
652	4.3 ± 0.4	BOTH			
667	4.3 ± 0.4	C.D.P.	4.4	0.12	LAVA
697	4.5 ± 0.4	SEMB.			
712	2.8 ± 0.4	BOTH			
847	2.3 ± 0.4	SEMB.			
892	2.5 ± 0.4	SEMB.	2.5	0.21	MESOZOIC SEDIMENTS
952	2.5 ± 0.4	SEMB.			

S.E. = standard error
S.D. = standard deviation
SEMB. = semblance
BOTH = C.D.P. and semblance

Some events corresponding to first refracted arrivals
were observed on some of the τ-p semblance plots. No
single , unique event could be seen to represent the
second arrival. In figure 25 the events marked b_1 ,b_2 and
b_3 appear with velocities 2.5 , 2.7 and 2.9 km/s respect-
ively. They are unlikely to represent real arrivals in
view of their large intercept times and are most probably
spurious effects due to the poor quality of the data. On
comparison with the original X-T data , no corresponding
events could be detected.

No other clearly defined events were distinguishable
on any of the plots. The event marked (c) in figure 25 is
probably a spurious effect produced by noise on the traces.
Certainly , it is unlikely that there would be any layers
of lower velocity beneath the Lewisian that would be visible
on a seismic record. This , and the fact that the event
appears to be an isolated occurence not appearing om any
other semblance plots , leads to the conclusion that it is
a spurious effect and should be treated as so in an inter-
pretation.

The values of stack in τ-p shown in figures 23 and 24 are
difficult to interpret as the data are so noisy. The ellipse
representing the reflection from the Lewisian is impossible
to detect amongst the noise although there is a local max-
imum in figure 24 at a p-value of about 0.4 ms/m (velocity=
2.4 km/s) and is labelled (b) in figure 25. This event
is probably spurious as it is more likely that event (a) is
real rather than event (b) in view of the large τ-value of
event (b) , and the fact that the velocity of (a) is nearer
to that to be expected for the Lewisian.

Figures 23, 24 and 25 are typical examples of the program outputs generated during this work. In most cases the data are of insufficient quality for interpretation from the τ-p plots of the types shown in figures 23 and 24 and velocities were picked from the semblance plots as shown in figure 25 or calculated from the C.D.P. gathers as shown in figure 22. Some typical plots of files up to number 562 are shown in figures 26-29. The axes, as on all the plots shown in this thesis, are as labelled in figures 23, 24 and 25.

From file 607 to file 697 there is a change in velocity of the first refracted arrival to a value of 4.4 km/s (see table 1). This is the region of the Minch fault zone. This normal fault forms the western boundary of the Sea of the Hebrides trough and divides the Lewisian from the Mesozoic rocks. The program outputs were studied to see if the effects of the fault were visible, but most of the files in this relatively small region were of too poor quality to yield any useful information. This was due to the overall low quality of the data and a reduction in the number of usable channels because of a change of recording tape. The first arrival on file 652 confirmed that the fault zone had been, or was being traversed and that refractions were now being detected from rocks within the trough.

From files 652 to 952 there appears to be three distinct velocities visible on the semblance plots. Files 652 to 697 show a series of events corresponding to refractions at velocities of 4.3 to 4.5 km/s. This event is best seen on the semblance plot of file 652 (figure 30). For comparison, figure 31 shows the value of stack in τ-p for the same file. It is apparent that there is an event with a p-value around 0.25 ms/m but the exact value is more difficult to pick.

The semblance plot of file 697 (figure 32) appears to show

all three of the events mentioned above. The 5.5 km/s arrival
is most probably a spurious effect because of its very early
arrival time which is inconsistent with the measured water depth
in that area. File 697 is the last file to show an event with
a velocity of 4.5 km/s. This event is probably a spurious effect
as implied by the large τ-value. Comparison with the X-T plot is
inconclusive to decide definitely. If the 5.5 km/s event is
ignored, it could conceivably have the following causes:

i) There is a compressed layer of Mesozoic rocks in this area
   produced by the movement in the fault zone.

ii) The underlying Torridonian (McQuillan and Binns, 1973) has
    outcropped in this locality through faulting.

iii) There has been an intrusion of Tertiary lava.

Of these, ii) and iii) seem most plausible. The observed
velocity of 4.4 km/s is reasonable for either model. Smythe and
Kenolty (1975) quote velocities of 4.1 and 3.6 km/s for lavas in
the area of the Sea of the Hebrides some 10 to 15 km northwest
of Canna, while the sections and maps given by McQuillan and
Binns (1973) suggest that Tertiary lavas are present in the
locality. For these reasons it seems more likely that lavas are
the more probable of the alternatives if the first arrival of
5.5 km/s is ignored.

After file 697, there are no more appearances of events with
velocities around 4.4 km/s, possibly suggesting that this loc-
ation marks the eastern boundary of the Minch fault zone. The
event (c) in figure 32 is spurious due to its large τ-value. Fig-
ures 33 and 34 compare both of Bowen's programs.

Although the aliased trajectory indicated in figure 33 is supp-
ressed in the anti-alias plot, there is no other apparent in-
terpretational advantage in using the more sophisticated and
computationally more time-consuming program with data of this
quality.

From files 697 to 952 (the last to be processed) the first refracted arrival appears with a velocity in the range 2.3 to 2.8 km/s, which is the result to be expected for Mesozoic rocks (Smythe and Kenolty, 1975). The large τ-values mean that these events are probably spurious. Typical examples of the plots obtained in this region are shown in figures 35 to 39 with similar p-valued events indicated.

No further events are clearly seen below the Mesozoic and the strong reflections and moderate to low velocities agree with the results of Binns et al (1974).

FIG 26

RAY PARAMETER
STACK FØR
NTAU= 188
.NP= 29

LINE 7 FILE 427

LINE 7 FILE 452

FIG.27

0

p

0·67

tau

4 sec

FIG.28
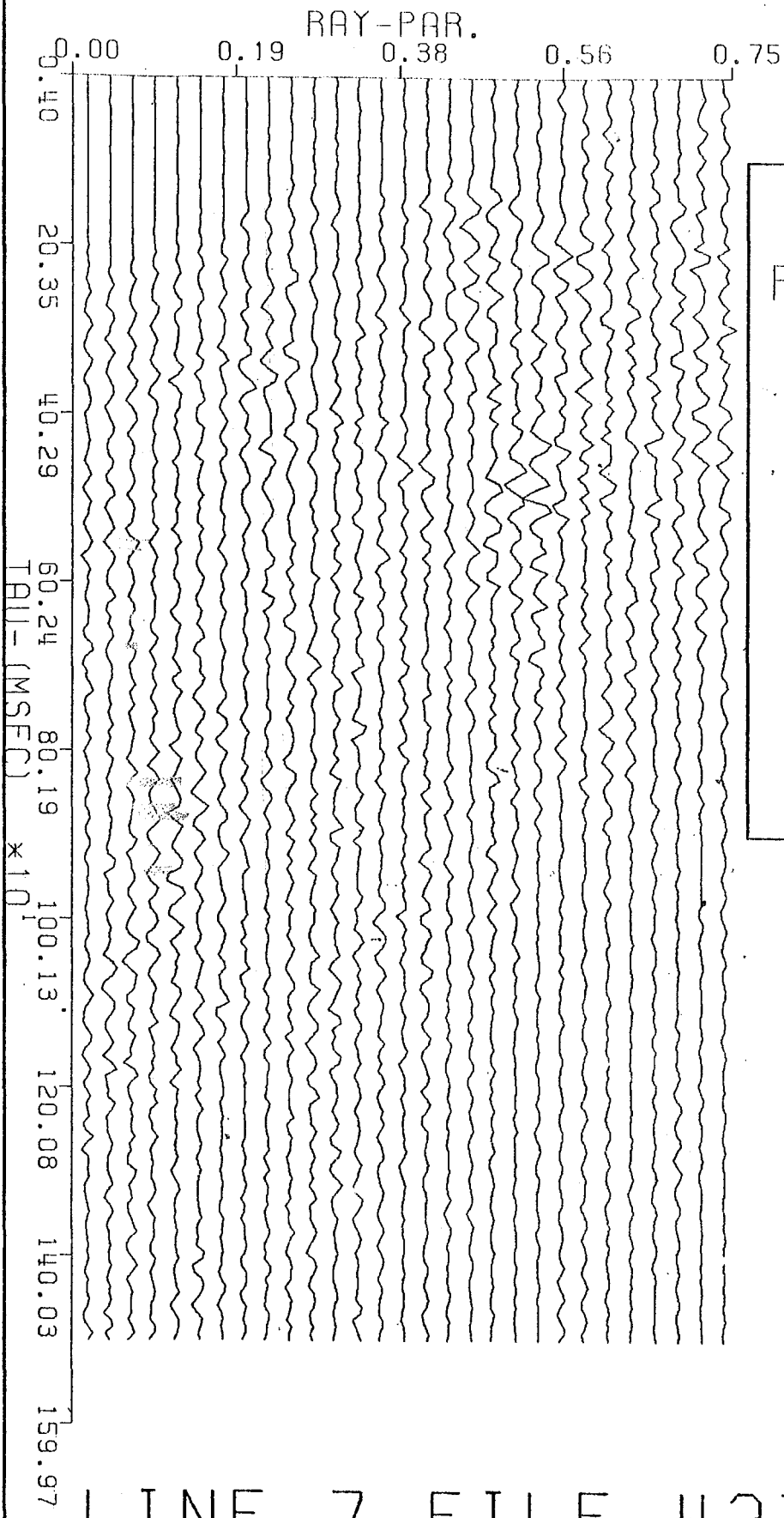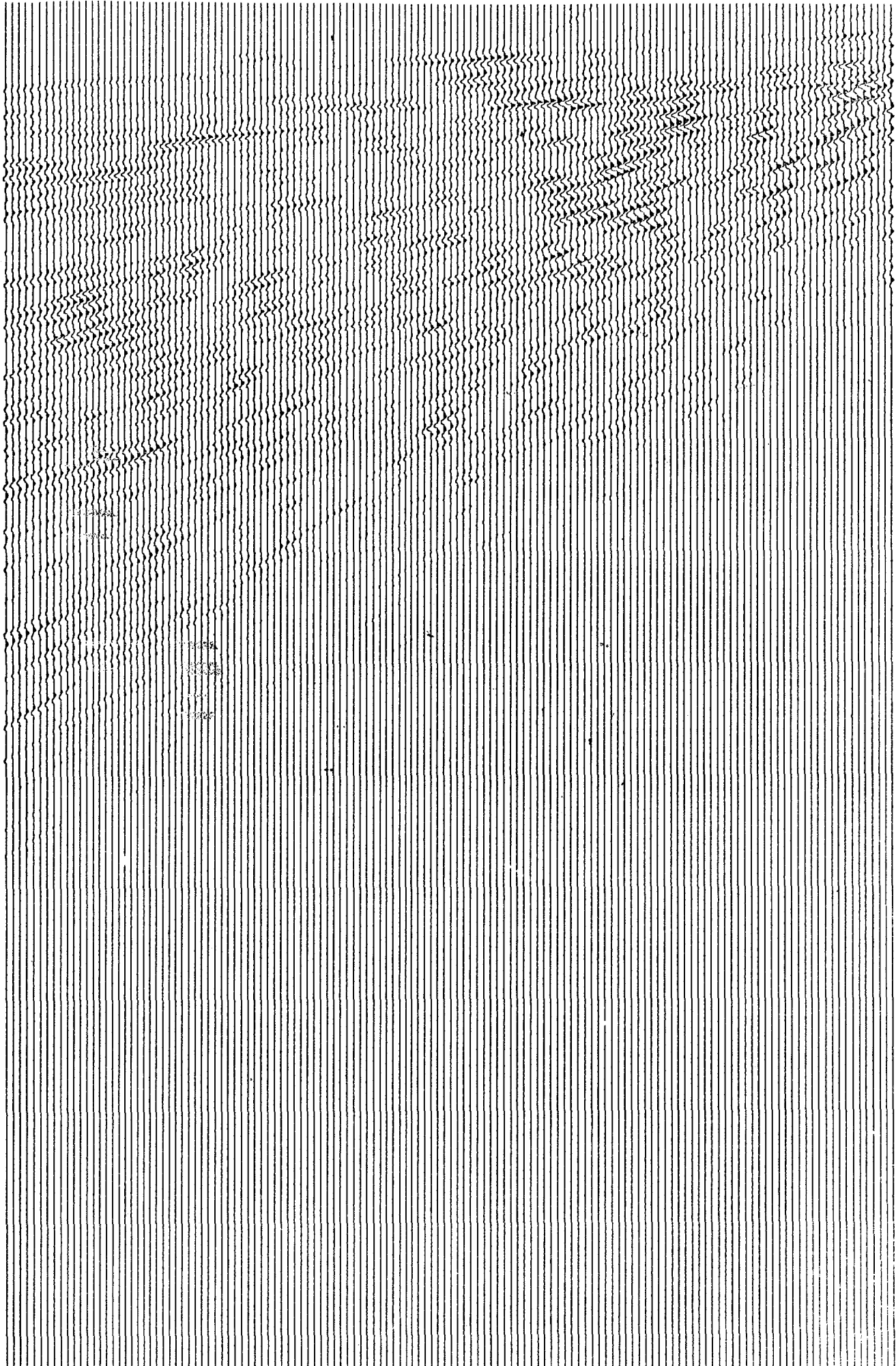
0   p   0·67
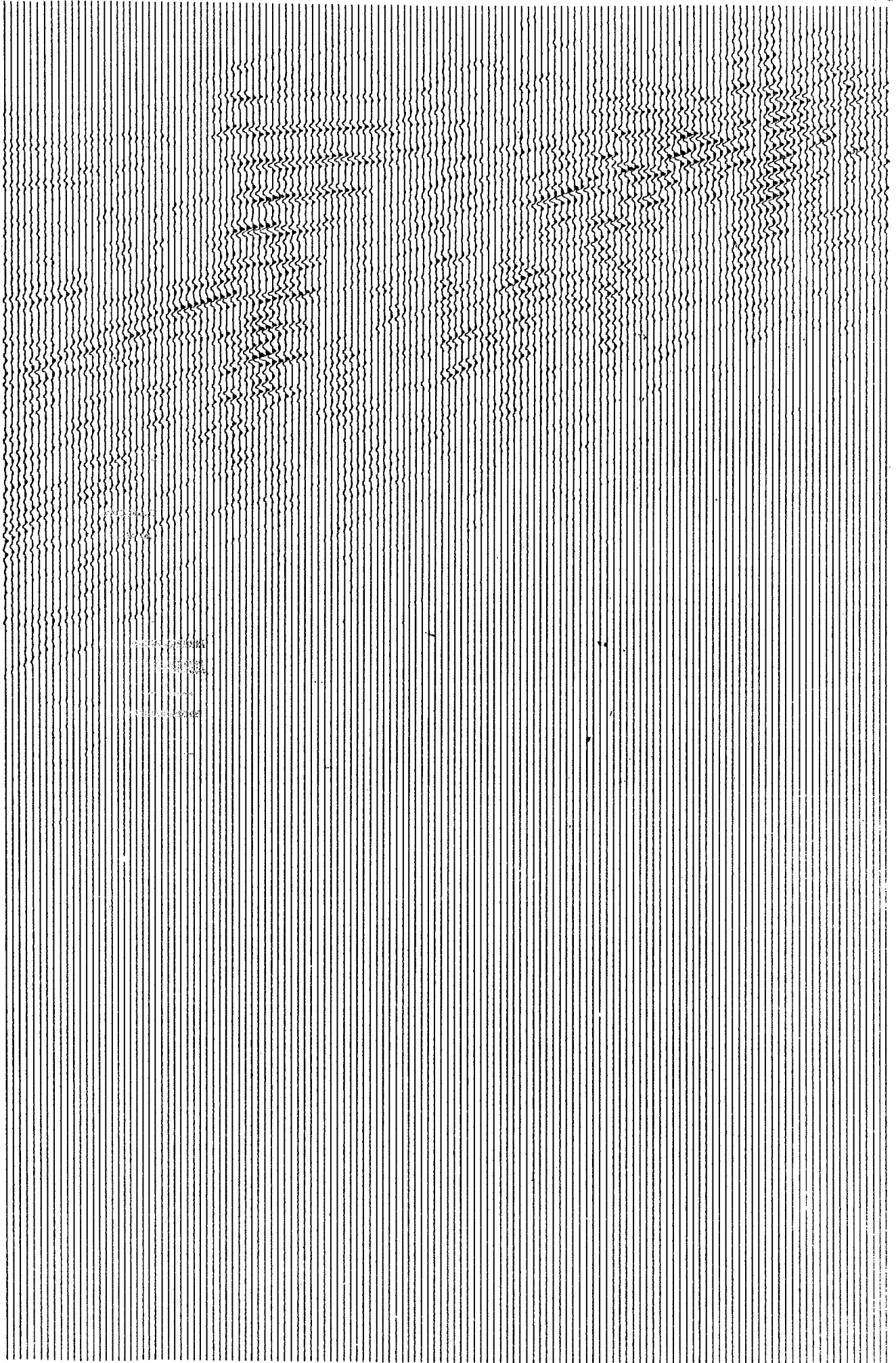
tau

4 sec

Line 7 · File 562

Velocity = 5·8 km/s
(assuming no dip)
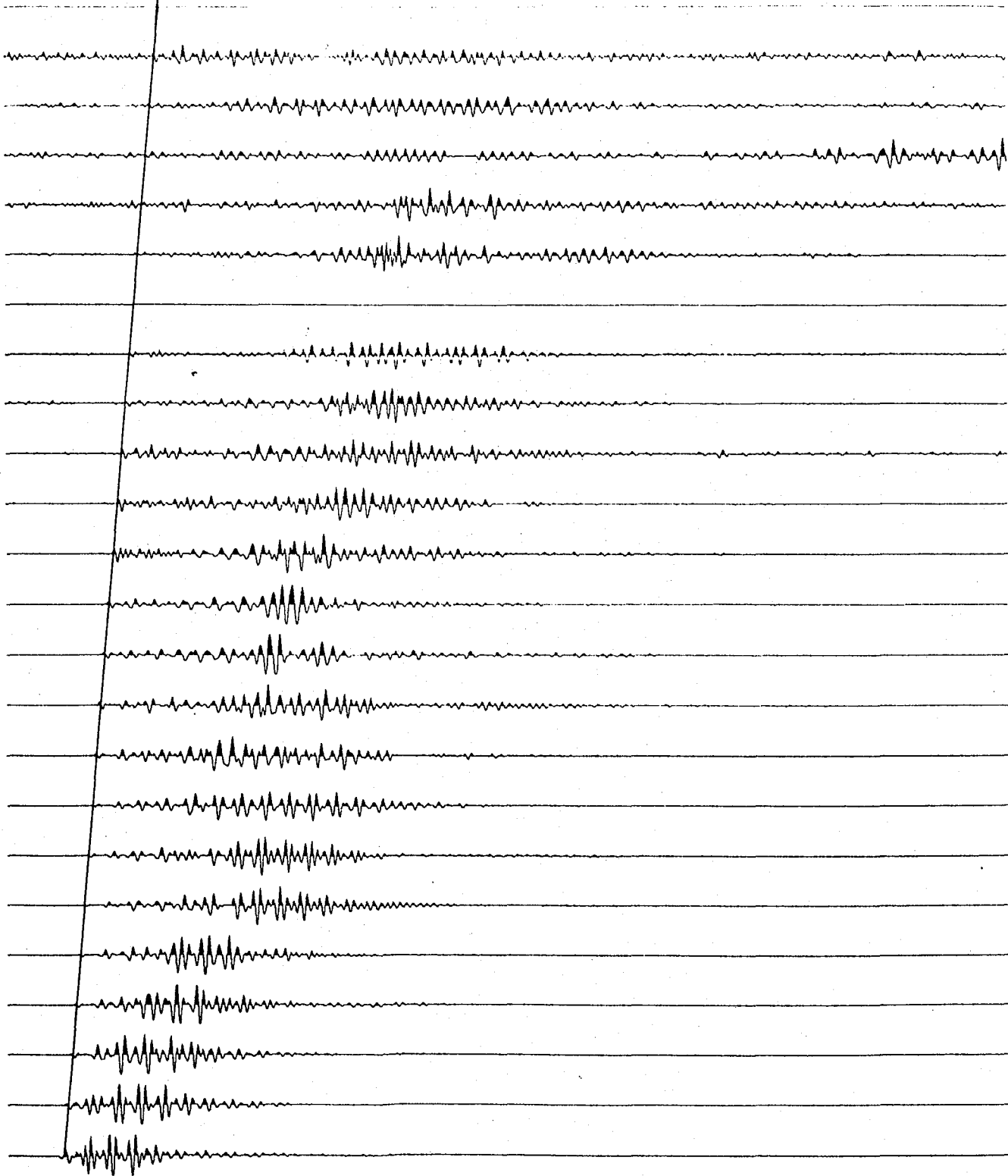
FIG.29
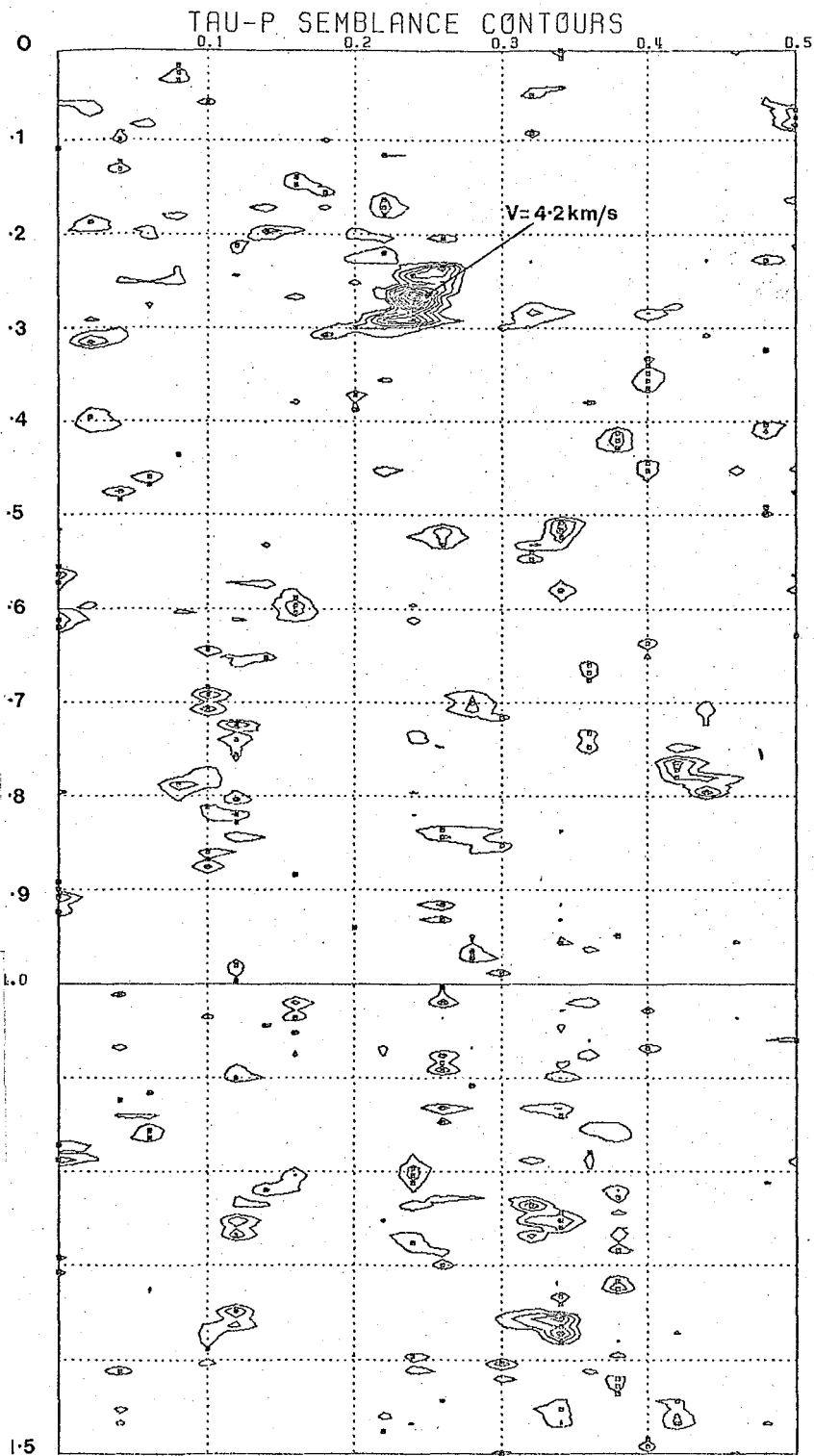
TAU-P SEMBLANCE CONTOURS

V = 4·2 km/s

FIG.31

LINE 7 FILE 652

RAY-PAR.

RAY PARAMETER STACK FØR NTAU= 188 NP= 26

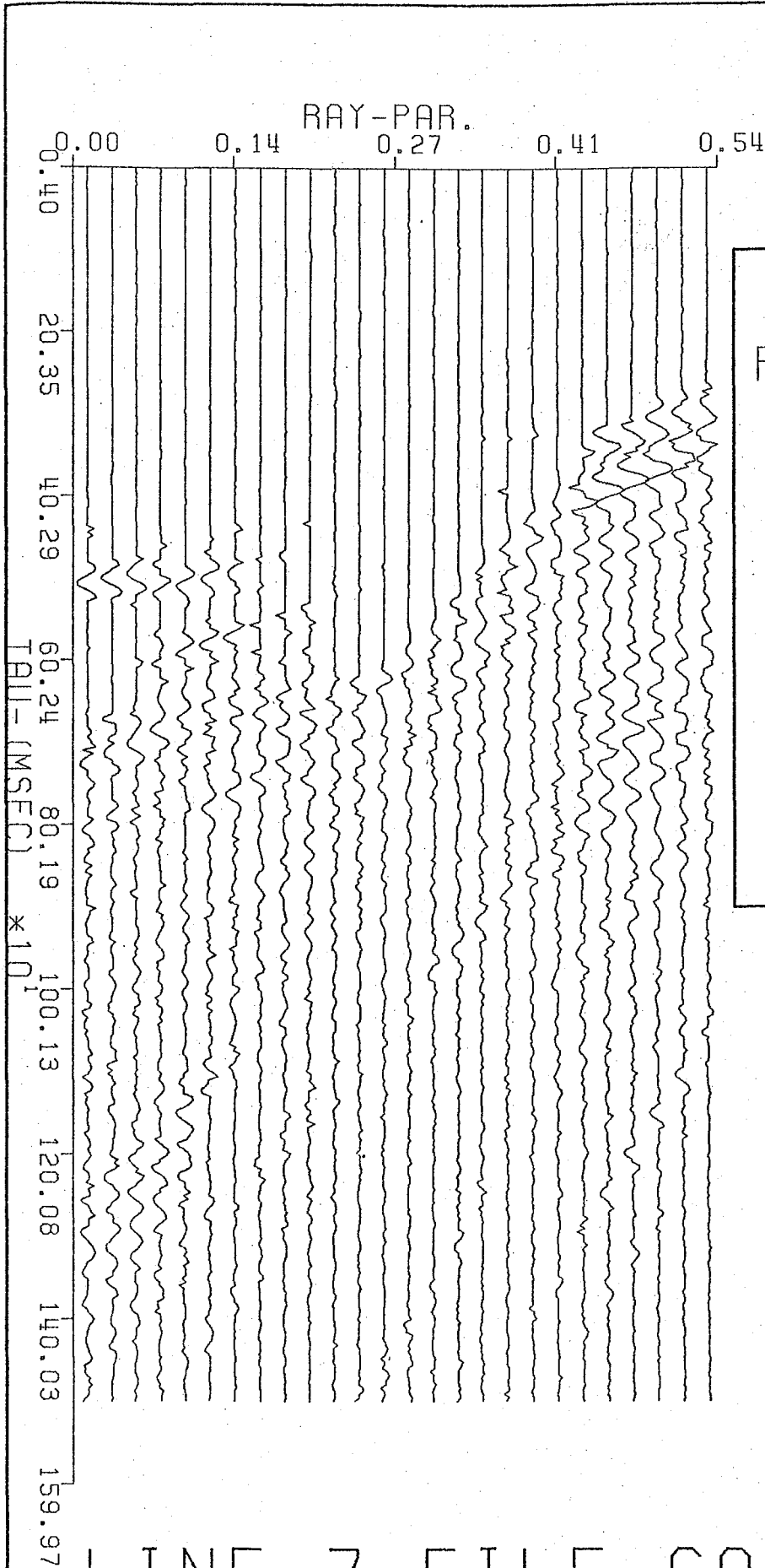TAU- (MSEC) *10¹

TAU-P SEMBLANCE CONTOURS

V≈5·6km/s

V≈4·5km/s

V≈2·4km/s

NO. OF CHANNELS = 24
SAMPLES PER CHANNEL = 102¹
SAMPLE DELAY = 0
LEVEL OF INTERPOLATION =
CHANNEL 1 OFFSET = 245.0
CHANNEL SPACING = 100.0
SAMPLING INTERVAL MS = 4
START OF ANALYSIS MS = 4
END OF ANALYSIS MS = 1500
TIME STEP MS = 8
OPERATOR GATEWIDTH MS =8
START RAY PAR. S/KM = 0.0(
END RAY PAR. S/KM = 0.50
RAY PAR. STEP S/KM = 0.02
MIN. CONTOUR VALUE = 0.10
CONTOUR INTERVAL = 0.05

FIG.33

RAY-PAR.

aliased trajectory

RAY PARAMETER
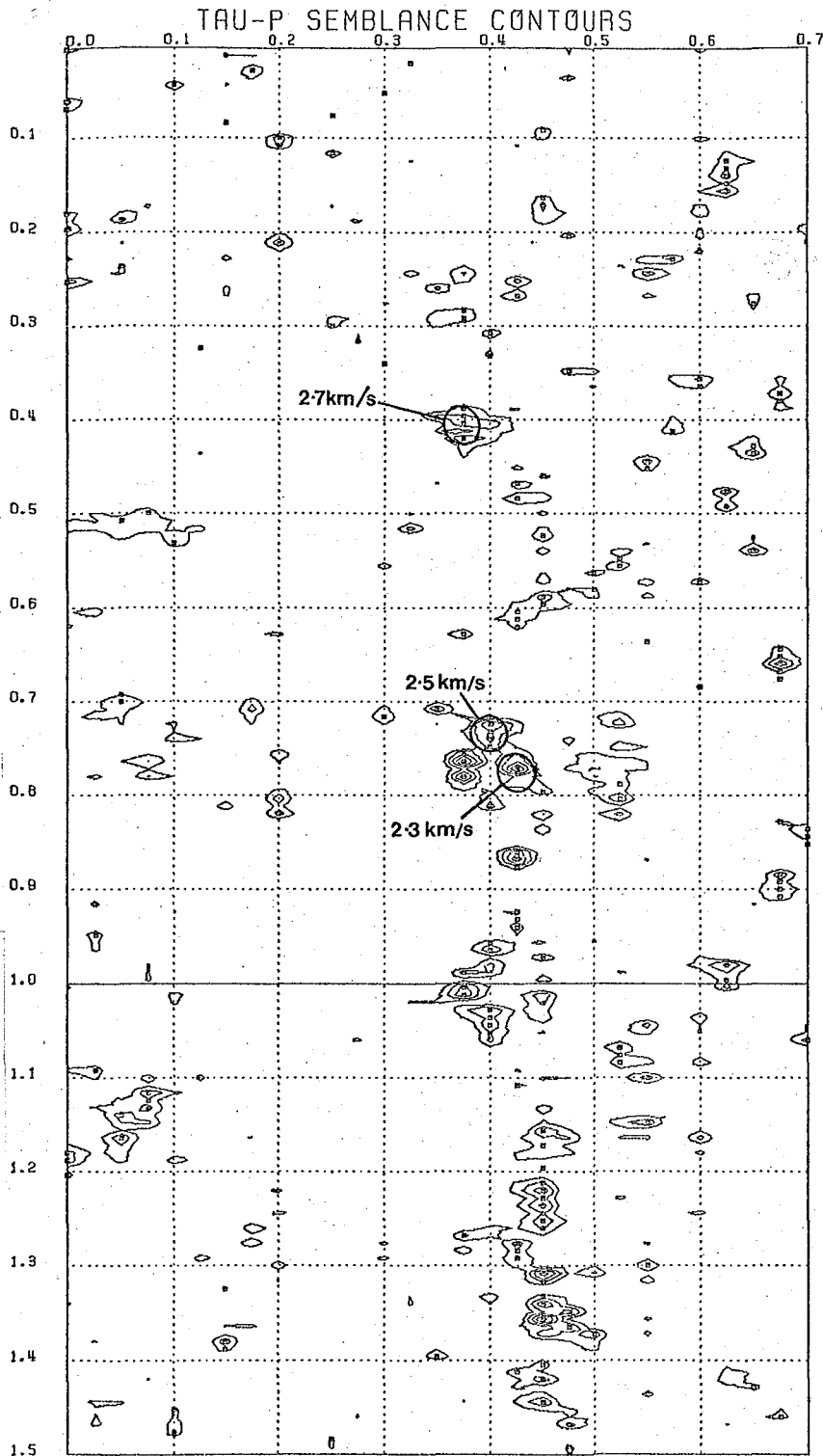
STACK FØR

NTAU= 188

NP= 26

TAU- (MSEC) *10¹

LINE 7 FILE 697

FIG.34
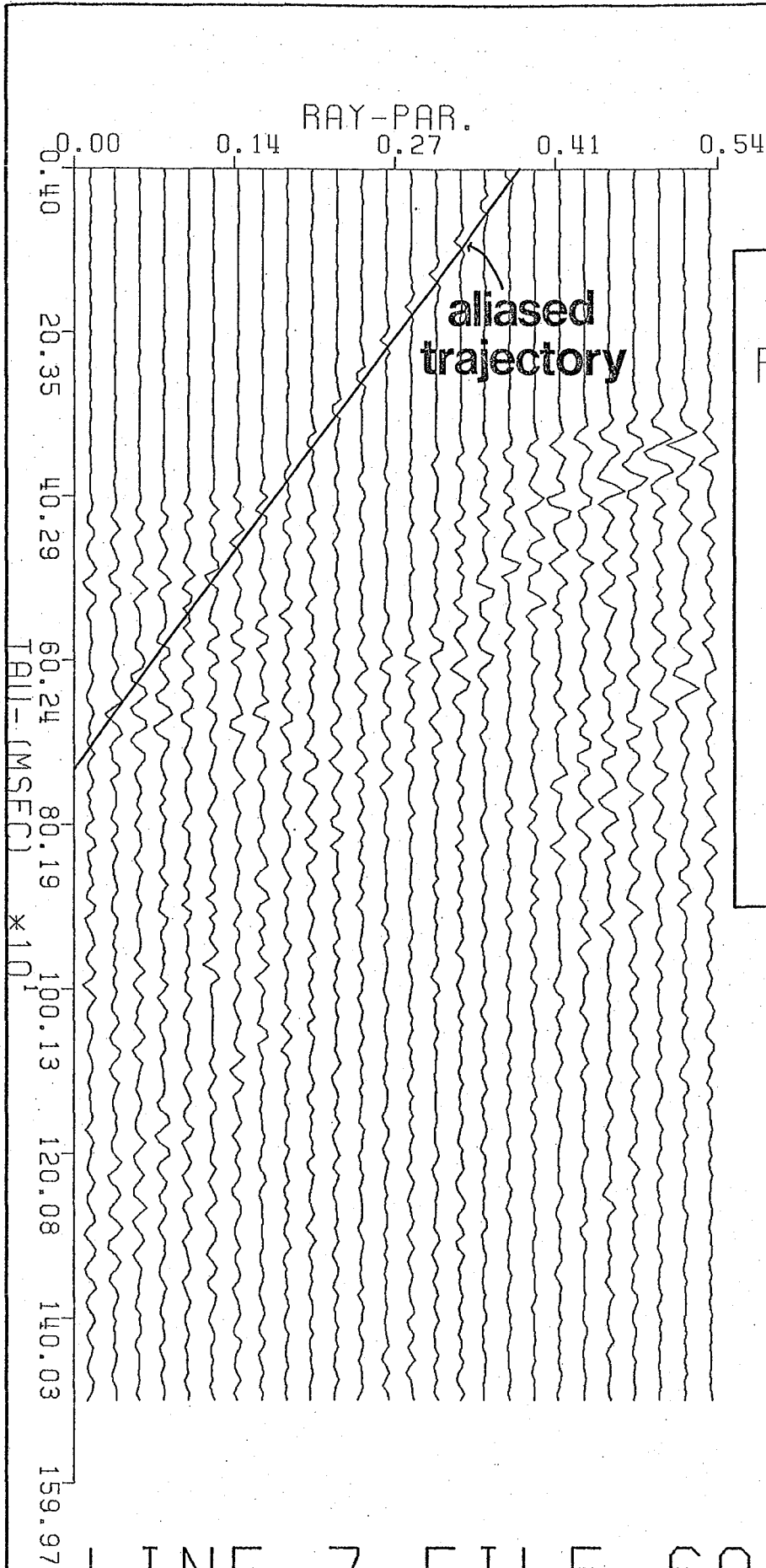
RAY PARAMETER STACK FØR

NTAU= 375

NP= 26

ANTI-ALIAS PARAMETERS:

SCAN:

3 CHANNELS

STEP SIZE:

1 CHANNELS

LINE 7 FILE 697

TAU-P SEMBLANCE CONTOURS

2·7km/s

2·5 km/s

2·3 km/s

TAU-P SEMBLANCE CONTOURS

2·7km/s

PROCESSING PARAMETERS
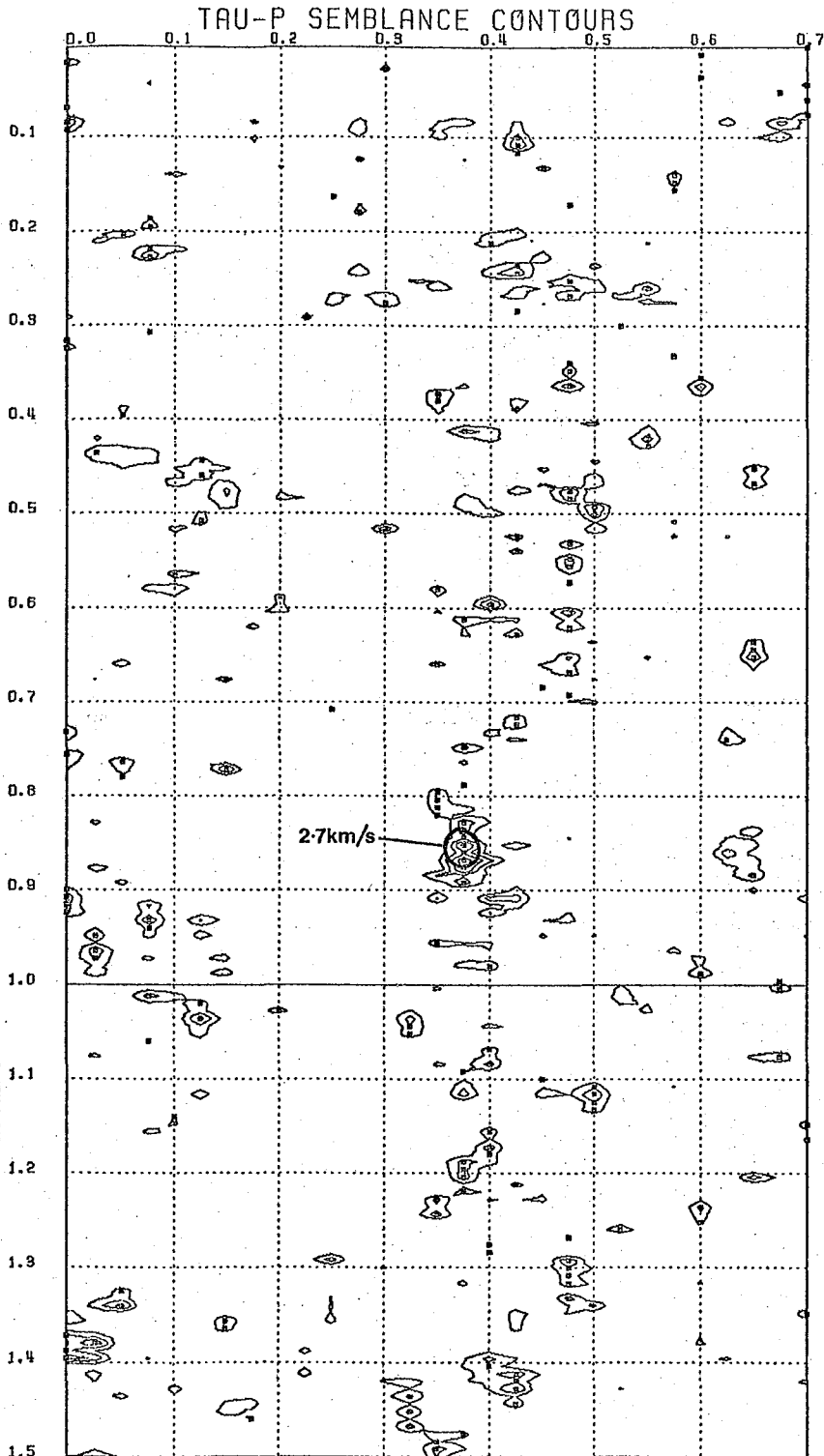
NO. OF CHANNELS = 24
SAMPLES PER CHANNEL = 102
SAMPLE DELAY = 0
LEVEL OF INTERPOLATION =
CHANNEL 1 OFFSET = 245.0
CHANNEL SPACING = 100.0
SAMPLING INTERVAL MS = 4
START OF ANALYSIS MS = 4
END OF ANALYSIS MS = 1500
TIME STEP MS = 8
OPERATOR GATEWIDTH MS =8
START RAY PAR. S/KM = 0.0
END RAY PAR. S/KM = 0.70
RAY PAR. STEP S/KM = 0.03
MIN. CONTOUR VALUE = 0.10
CONTOUR INTERVAL = 0.05

FIG.37

RAY-PAR.

RAY PARAMETER STACK FØR

NTAU= 188

NP= 29

TAU- (MSEC) *10¹

LINE 7 FILE 847

TAU-P SEMBLANCE CONTOURS

PROCESSING PARAMETERS

NO. OF CHANNELS = 24
SAMPLES PER CHANNEL = 10
SAMPLE DELAY = 0
LEVEL OF INTERPOLATION =
CHANNEL 1 OFFSET = 245.0
CHANNEL SPACING = 100.0
SAMPLING INTERVAL MS = 4
START OF ANALYSIS MS = 4
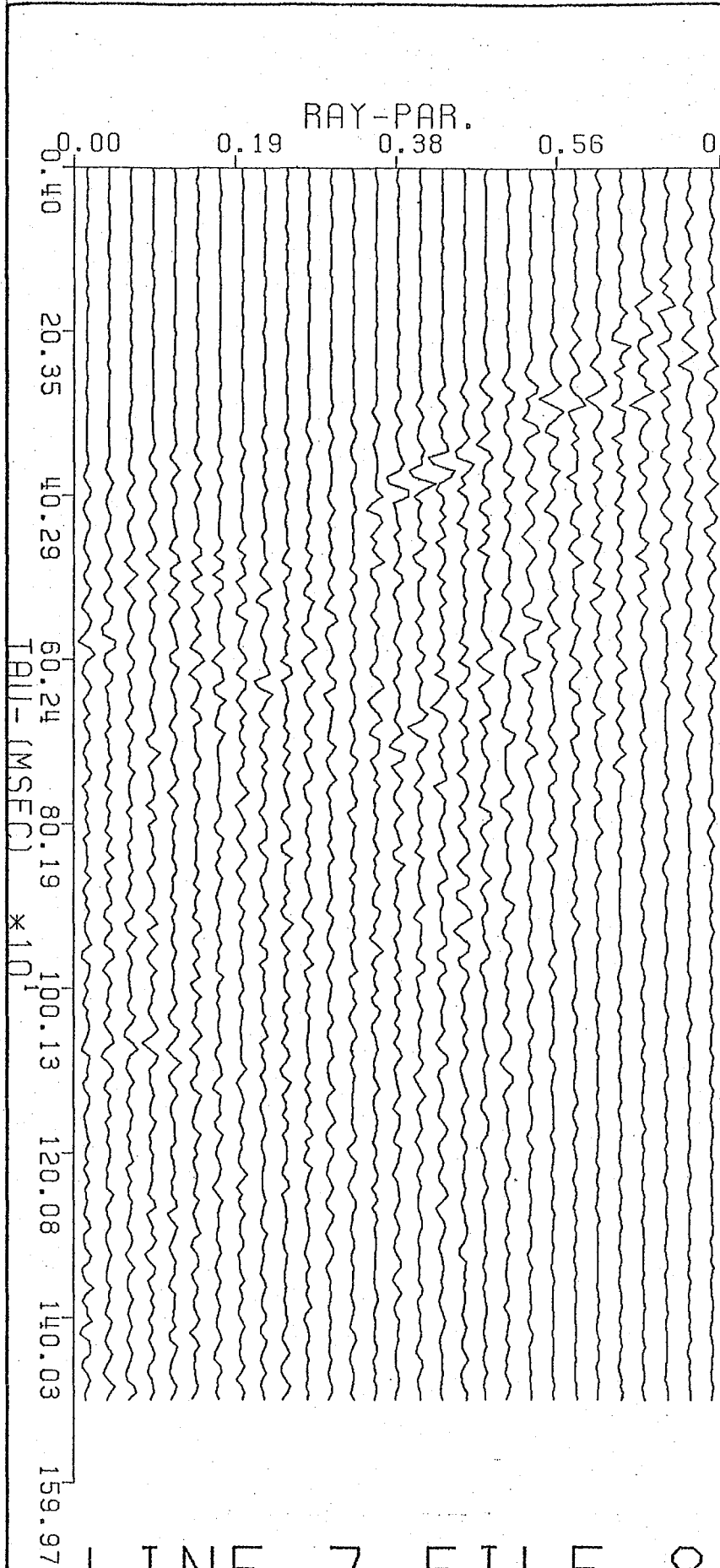END OF ANALYSIS MS = 150
TIME STEP MS = 8
OPERATOR GATEWIDTH MS =8
START RAY PAR. S/KM = 0.
END RAY PAR. S/KM = 0.70
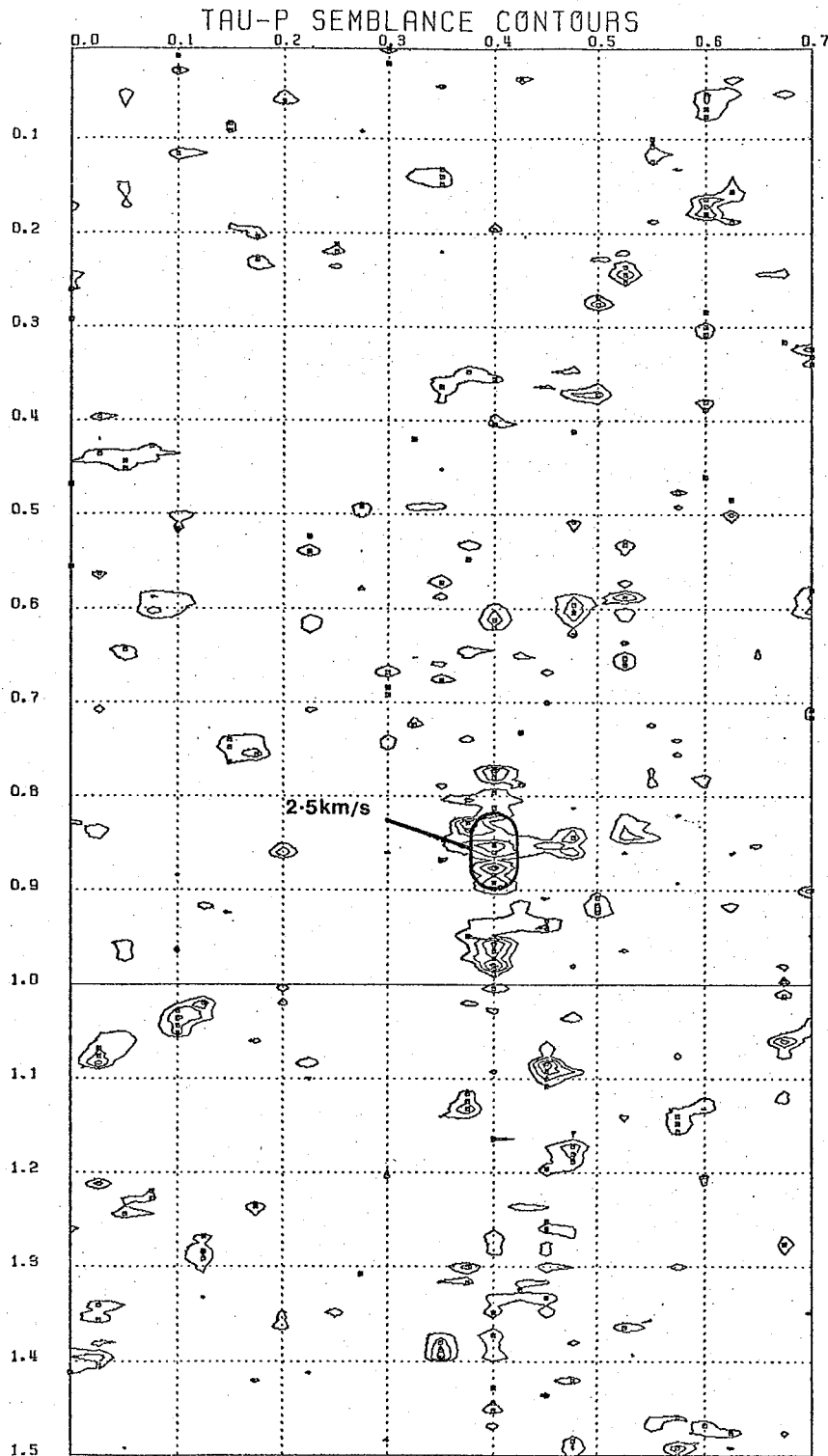RAY PAR. STEP S/KM = 0.0
MIN. CONTOUR VALUE = 0.1
CONTOUR INTERVAL = 0.05

FIG.39

RAY-PAR.
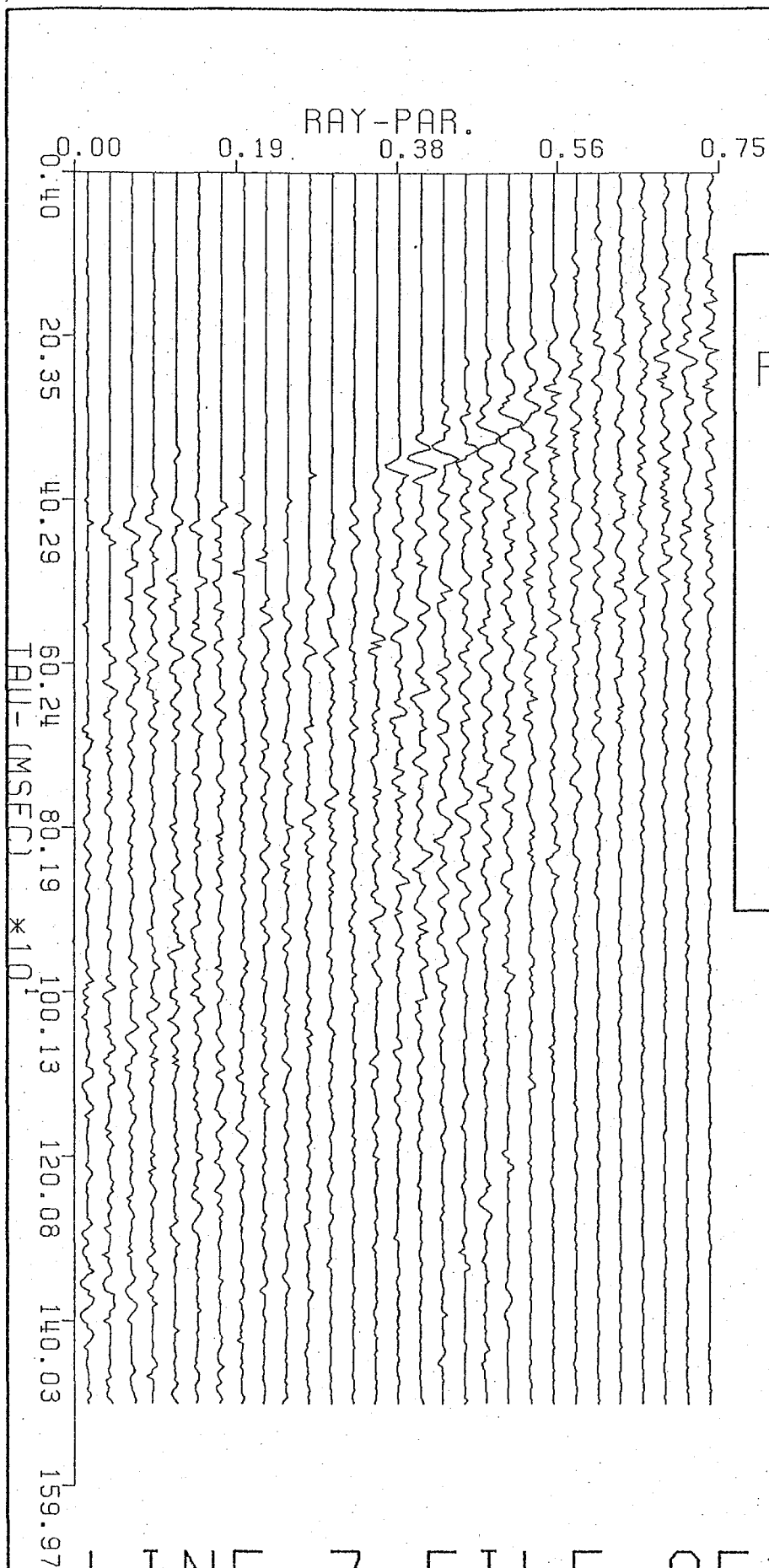
0.00   0.19   0.38   0.56   0.75

TAU- (MSEC) *10

0.40 20.35 40.29 60.24 80.19 100.13 120.08 140.03 159.97

RAY PARAMETER
STACK FØR
NTAU= 375
NP= 29

ANTI-ALIAS
PARAMETERS:

SCAN:
3 CHANNELS

STEP SIZE:
1 CHANNELS

LINE 7 FILE 952

5.3.2.   Line 9

Data were processed from file 277 to file 652 so as to include the Torridonian and Mesozoic rocks (figure 18). Velocity analysis was performed on every fifteenth file and the average dip for the file was calculated and corrected for, as for line 7.   The overall quality of the data from line 9 was poorer than from line 7 and the number of C.D.P. gathers of sufficient quality that were obtained was only fourteen. An example is shown in figure 40.   All the results obtained are summarised in table 2.   All of the τ-p semblance plots were noisy, and the first refracted events were indiscernable. Figure 41 shows a typical example.   The events lying between p = 0·60 to 0·70 ms/m represent the direct water wave, but other events are difficult to identify.   The events with p-values of 0·40 ms/m and 0·17 ms/m may be due to refractions or merely spurious effects - it is impossible to say which.

From file 277 to file 502, the velocity of the first refracted arrival is relatively constant and has an average value of 4·6 km/s. This is interpreted as being the velocity of the Torridonian and is in fair agreement with the value of 4·8 km/s quoted by Smythe et al (1972) for the Torridonian around northern Skye, and by Summers (pers. comm.).

The data from file 577 to file 652 are of particularly bad quality. Several changes of recording tape and the excessive noise from glitches rendered the majority of even the C.D.P. gathers completely useless for interpretation.   The only two files that could be interpreted gave velocities for the first refracted arrival as 2·4 km/s and 3·9 km/s. The former result agrees with the value of velocity calculated for the Mesozoic rocks in line 7, but the latter result does not.   The composition and velocity of the Mesozoic rocks may well differ between the area around line 9 and around line 7, and there is no reason to assume that the velocities will agree exactly.   Nevertheless, the value of 3·9 km/s

TABLE 2

FILE	VELOCITY±S.E. OF FIRST ARRIVAL(km/s)	OBTAINED FROM:	AVERAGE VELOCITY (km/s)	S.D. (km/s)	ROCK TYPE
277	4.6 ± 0.4	C.D.P.			
292	4.9 ± 0.4	C.D.P.			
307	4.6 ± 0.4	C.D.P.			
322	4.1 ± 0.4	C.D.P.			
337	4.9 ± 0.4	C.D.P.			
397	4.4 ± 0.4	C.D.P.	4.6	0.30	TORRID-ONIAN
412	4.4 ± 0.4	C.D.P.			
427	4.1 ± 0.4	C.D.P.			
442	4.4 ± 0.4	C.D.P.			
457	4.9 ± 0.4	C.D.P.			
487	4.9 ± 0.4	C.D.P.			
502	4.4 ± 0.4	C.D.P.			
577	3.9 ± 0.4	C.D.P.	−	−	MESOZOIC SEDIMENTS (?)
592	2.4 ± 0.4	C.D.P.			

S.E. = standard error
S.D. = standard deviation

seems inordinately high but because of the lack of good data, reasonable interpretation is impossible. The discrepancy may be due to geological reasons, but is more likely to be merely a reflection of the poor quality of the data and the ambiguity of choosing the first refracted event on the C.D.P. gather, particularly as the amplitude of this event is considerably smaller than the subsequent arrivals further down the trace. These will tend to swamp the first arrival when the normalisation process is applied.

Second refracted arrivals were impossible to discern on all the files along line 9.

As with line 7, the quality of the data has been insufficient for interpretation to be made with the τ-p method alone, and with the lowest quality data the method has been completely impotent. Figure 42 is a typical example. Only the simplest of interpretations has been presented since any further detail is unjustified.

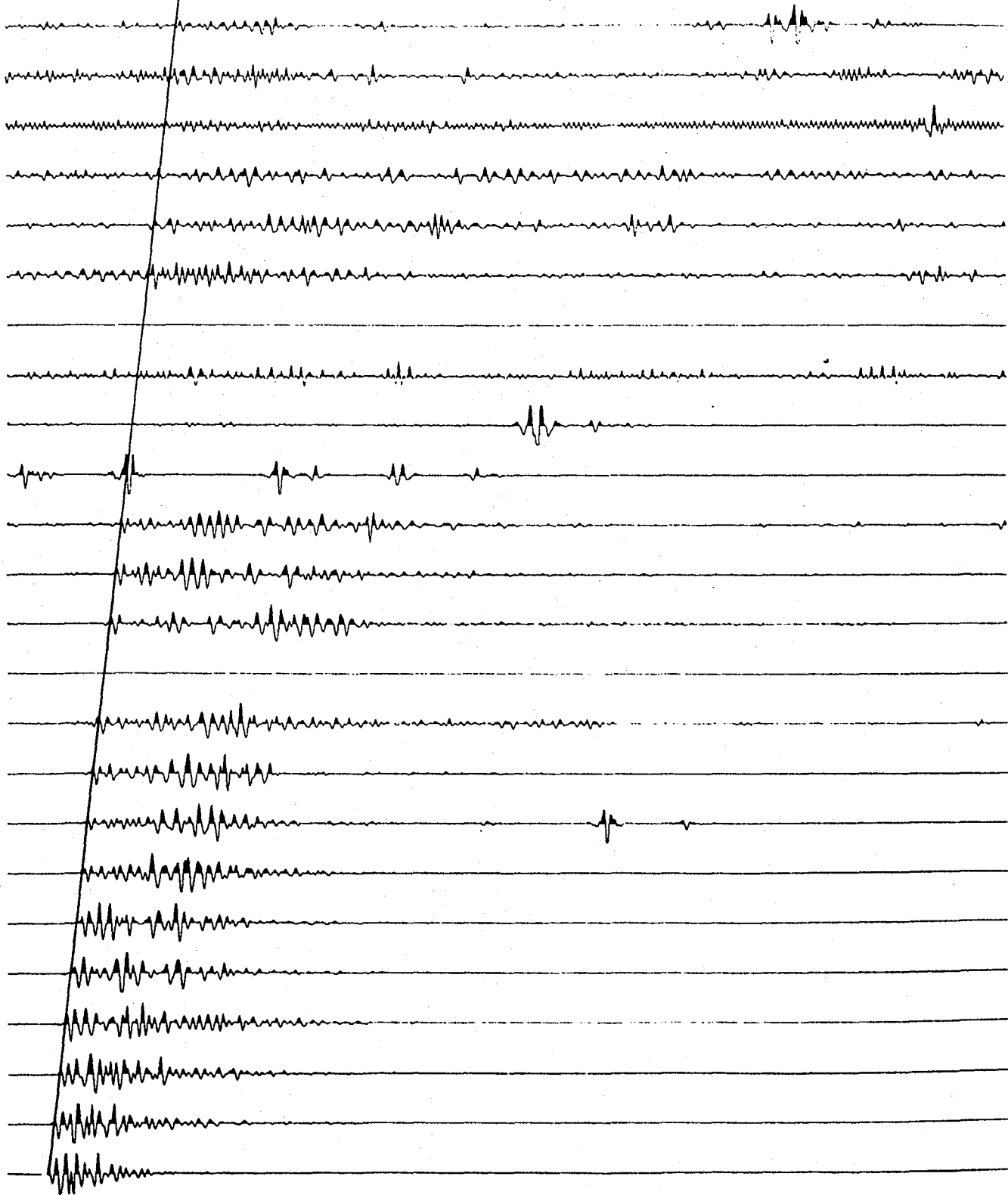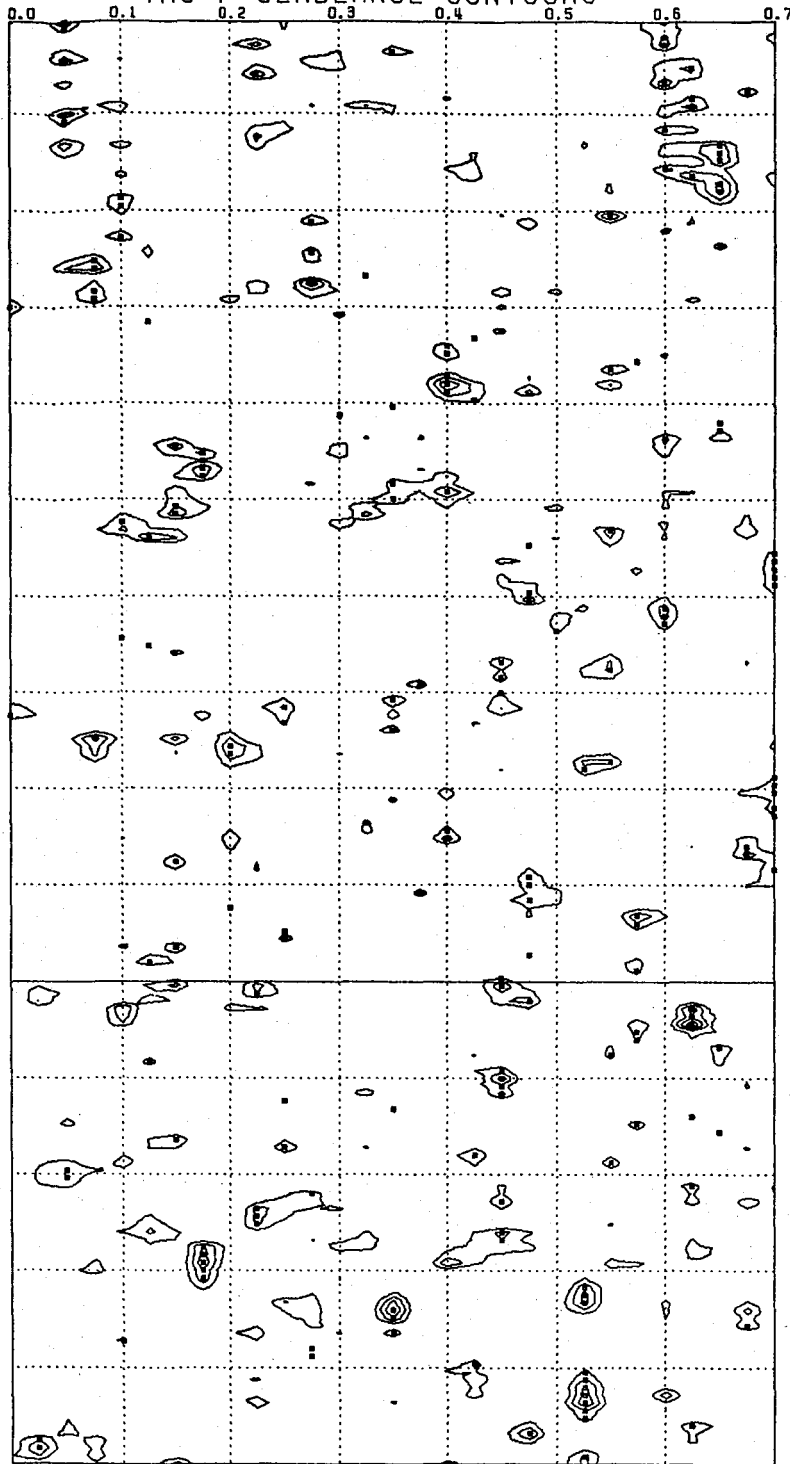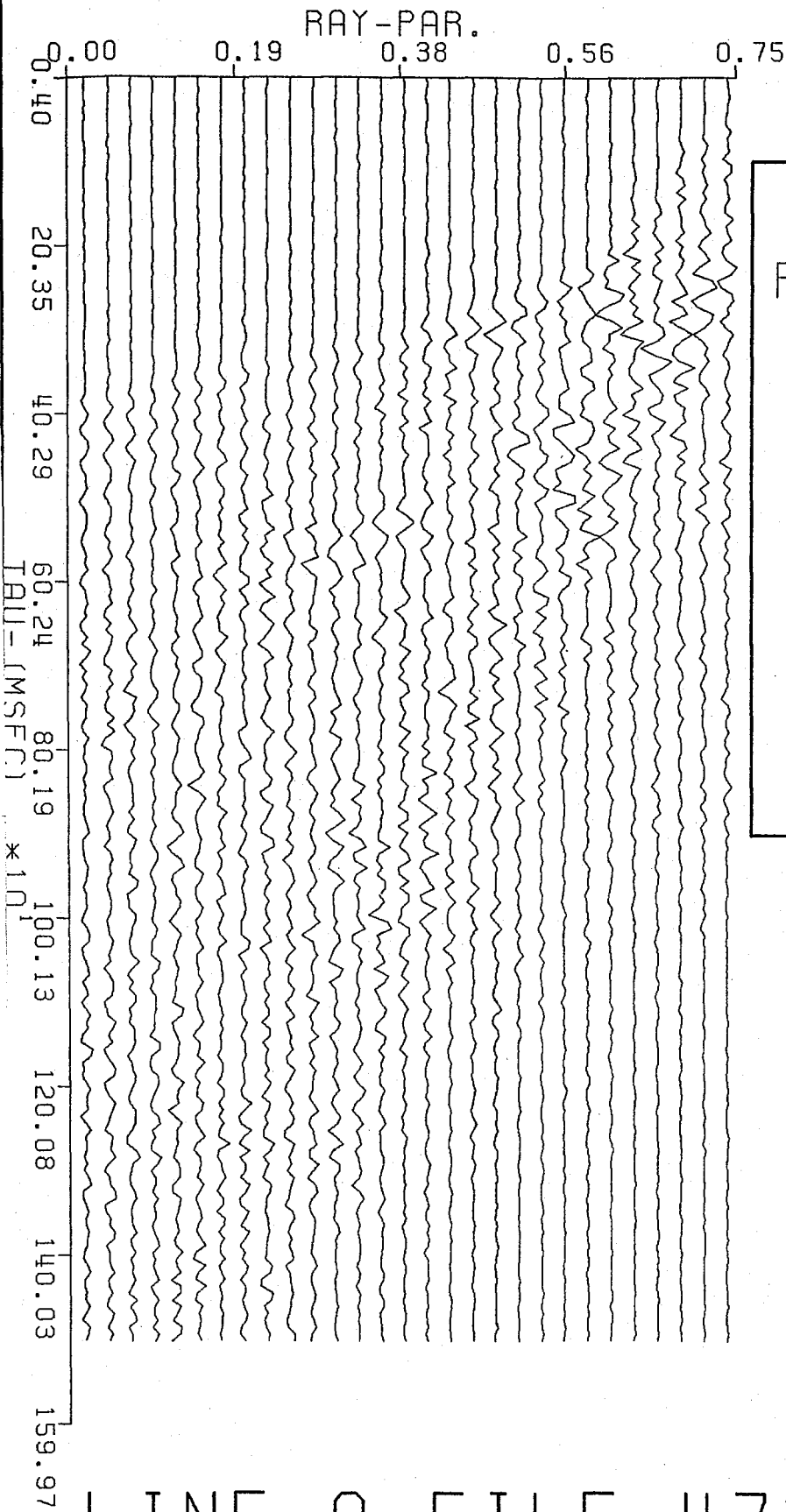Line 9   File 412

Velocity = 4·4 km/s
(after dip correction)

FIG.40

TAU-P SEMBLANCE CONTOURS

PROCESSING PARAMETERS

NO. OF CHANNELS = 24
SAMPLES PER CHANNEL = 1024
SAMPLE DELAY = 0
LEVEL OF INTERPOLATION = 1
CHANNEL 1 OFFSET = 245.0
CHANNEL SPACING = 100.0
SAMPLING INTERVAL MS = 4
START OF ANALYSIS MS = 4
END OF ANALYSIS MS = 1500
TIME STEP MS = 8
OPERATOR GATEWIDTH MS =8
START RAY PAR. S/KM = 0.00
END RAY PAR. S/KM = 0.70
RAY PAR. STEP S/KM = 0.03
MIN. CONTOUR VALUE = 0.10
CONTOUR INTERVAL = 0.05

FIG.42

RAY-PAR.

RAY PARAMETER
STACK FØR
NTAU= 188
NP= 29

LINE 9 FILE 472

CONCLUSION

The purposes of this work were to investigate the velocity structure of regions in the Sea of the Hebrides and to determine whether or not the T-p transform is applicable to the interpretation. The velocity structure was determined and appears generally to be consistent with previous work, although some slight differences are apparent. It was found the the T-p transformation was of seriously limited practical applicability for this work because of the quality of the data. Noisy channels, due to equipment failure, and the limited offset rendered the T-p transformation wholly inappropriate and recourse to simpler, conventional methods of interpretation was found necessary. However, the usefulness of the transformation should not be judged solely on the results obtained in this work. With better quality data, it may prove to be useful not only in interpretation but also in processing routines as mentioned briefly by McMechan and Ottolini (1980). A way of utilising the transform is to apply it in the normal way to X-T data, then to remove the unwanted, spurious effects such as aliasing and finally to apply the transformation to the T-p data in reverse to recover the original X-T data. In this way the final signal to noise ratio should be increased, since the T-p data set facilitates the partial separation of pure signal from noise. This process is currently being investigated in industry and appears to be successful in improving the quality of C.D.P. gathers before they are stacked.

APPENDIX A

REFERENCES

Backus, G., and Gilbert, J.F., 1967, Numerical application of a formalism for geophysical inverse problems, Geophys. J.R. astron. Soc., 13, 247 - 276.

Bates, A.C., and Kanasewich, E.R., 1976, Inversion of seismic travel times using the Tau method, Geophys.J.R. astron. Soc., 47, 59 - 72.

Bessonova, E.N., Fishman, V.M., Ryaboyi, V.A., and Sitnikova, G.A., 1974, The Tau method for inversion of travel times -1 : Deep seismic sounding data, Geophys. J.R. astron. Soc., 36, 377 - 398.

Bessonova, E.N., Fishman, V.M., and Sitnikova, G.A., 1970, Determination of the limits for velocity distributions from discrete travel time observations, Paper presented at the 7th Upper Mantle Symposium on Geophysical Theory and Computers, Södergarn, Sweden.

Binns, P.E., McQuillan, R., and Kenolty, N., 1974, The geology of the Sea of the Hebrides, Rep. no. 73/14, Inst. Geol. Sci., H.M.S.O.

Bowen, A.N., 1980, An investigation into the tau-p mapping, M.Sc. thesis, University of Durham (unpubl.).

Brune, J.N., 1964, Travel times, body waves, and the normal modes of the earth, Bull. seismol. Soc. Am., 2099 - 2128.

Bullen, K.E., 1963, Introduction to the theory of seismology, University Press, Cambridge.

Diebold, J.B., and Stoffa, P.L., 1979, The traveltime equation, tau-p mapping, and inversion of common mid-point data, Geophysics, 46, no. 3, 238 - 254.

Gerver, M.L., and Markushevich, V.M., 1966, Determination of seismic wave velocity from the travel time curve, Geophys. J.R. astron. Soc., 11, 165 - 173.

Gerver, M.L. and Markushevich, V.M., 1967, On the characteristic properties of traveltime curves, Geophys. J.R. astron. Soc., 13, 241 - 246.

Hall, J., and Al-Haddad, F.M., 1976, Seismic velocities in the Lewisian metamorphic complex, northwest Britain - 'in situ' measurements, Scott. J. Geol., 12, no. 4, 305 - 314.

Harker, A., 1941, The West Highlands and The Hebrides, University Press, Cambridge.

Henry, M., and Orcutt, J.A., 1980, A new method for slant stacking refraction data, Geophys. Res. Lett. Washington., 7, no. 12, 1073 - 1076.

Herglotz, G., 1907, Über das benndorfsche problem der fortflanzungs-geshwindig beit der erdbebenstrahlin, Phys. Z., 8, 145 - 147.

Johnson, L.E., and Gilbert, F., 1972, A new datum for use in the body wave travel time inverse problem, Geophys. J.R. astron. Soc., 30, 373 - 380.

Kennett, B.L.N., 1977, The inversion of reflected wave travel times, Geophys. J.R. astron. Soc., 49, 739 - 746.

Mayne, W.H., 1962, Common reflection point horizontal stacking techniques, Geophysics, 27, 927 - 938.

McMechan, G.A., and Ottolini, R., 1980. Direct observation of a p-τ curve in a slant stacked wave field, Bull. seismol. Soc. Am., 70, no.3, 775 - 789.

McQuillan, R., and Binns, P.E., 1973, Geological Structure in the Sea of the Hebrides, Nature (phys. Sci.), 241, 2 - 4.

Peach, B.N., and Horne, J., 1930, Chapters on the geology of Scotland, Oxford University Press.

Richey, J.E., and Thomas, H.H., 1930, The Geology of Ardnamurchan, North-West Mull and Coll, Mem. geol. Surv. Scotland, H.M.S.O.

Savit, C.H., 1977, Future trends in geophysical exploration : Oil and Gas J., 75, 129 - 132

Schultz, P.S., and Claerbout, J.F., 1978, Velocity estimation and downward continuation by wavefront synthesis, Geophysics, 43, no. 4, 691 - 714.

Smythe, D.K., and Kenolty, N., 1975, Tertiary Sediments in the Sea of the Hebrides, J. geol. Soc. London, 131, 227 - 233.

Smythe, D.K., Sowerbutts, W.T.C., Bacon, M., and McQuillan, R., 1972, Deep Sedimentary Basin below Northern Skye and the Little Minch, Nature (phys. Sci.), 236, 87 - 89.

Stoffa, P.L., and Buhl, P., 1980, Two-ship multichannel seismic experiments for deep crustal studies, J. geophys. Res., 84, 7645 - 7660.

Stoffa, P.L., Buhl, P., Diebold, J.B., and Wenzel, F., 1979, Direct mapping of seismic data to the domain of intercept time and ray parameter - a plane-wave decomposition, Geophysics, 46, no. 3, 255 - 267.

Taner, M.T., and Koehler, F., 1967, Velocity spectra - digital computer derivation and applications of velocity functions, Geophysics, 34, no. 6, 859 - 881.

Telford, W.M., Geldart, L.P., Sheriff, R.E., and Keys, D.A., 1976, Applied Geophysics, Cambridge University Press.

Wiechert, E., 1910, Bestimmung des weges der erdbebenwellen in erdinnern, 1. Theoretisches, Phys. Z., 11, 294 - 304.